Inorganic Chemistry

Trinuclear Nickel Complexes with Triplesalen Ligands: Simultaneous Occurrence of Mixed Valence and Valence Tautomerism in the Oxidized Species

Thorsten Glaser,*,[†] Maik Heidemeier,[†] Roland Fröhlich,[‡] Peter Hildebrandt,[§] Eberhart Bothe,[∥] and Eckhard Bill[∥]

Institut für Anorganische und Analytische Chemie, Westfälische Wilhelms-Universität Münster, Wilhelm-Klemm-Strasse 8, D-48149 Münster, Germany, Organisch-Chemisches Institut, Westfälische Wilhelms-Universität Münster, Corrensstr. 40, D-48149 Münster, Germany, Max-Volmer-Laboratorium, Technische Universität Berlin, Strasse des 17 Juni 135, D-10623 Berlin, Germany, and Max-Planck-Institut für Bioanorganische Chemie, Stiftsstr. 34-36, D-45470 Mülheim, Germany

The coordination chemistries of the triple tetradentate triplesalen ligands H_6talen, H_6talen$^{t-Bu_2}$, and H_6talen^{NO_2} have been investigated with nickel(II). These triplesalen ligands provide three salen-like coordination environments bridged in a *meta*-phenylene arrangement by a phloroglucinol backbone. The structures of the complexes [(talen)Ni$^{II}_3$], [(talen$^{t-Bu_2}$)Ni$^{II}_3$], and [(talen^{NO_2})Ni$^{II}_3$] have been determined by single-crystal X-ray diffraction. All three compounds are composed of neutral trinuclear complexes with square-planar coordinated Ni^{II} ions in a salen-like coordination environment. Whereas the overall molecular structure of [(talen^{NO_2})Ni$^{II}_3$] is nearly planar, the structures of [(talen)Ni$^{II}_3$] and [(talen$^{t-Bu_2}$)Ni$^{II}_3$] are bowl-shaped as a result of ligand folding. The strongest ligand folding occurs at the central nickel–phenolate bond of [(talen$^{t-Bu_2}$)Ni$^{II}_3$], resulting in the formation of a chiral hemispherical pocket. The dependence of the physical properties by the substituents on the terminal phenolates has been studied by FTIR, resonance Raman, UV–vis–NIR absorption, and electrochemistry. The three nickel–salen subunits are electronically interacting via the π system of the bridging phloroglucinol backbone. The strength of this interaction is mediated by two opposing effects: the electron density at the terminal phenolates and the folding of the ligand at the central phenolates. The parent complex [(talen)Ni$^{II}_3$] is irreversibly oxidized at 0.32 V versus ferrocenium/ferrocene (Fc$^+$/Fc), whereas [(talen$^{t-Bu_2}$)Ni$^{II}_3$] and [(talen^{NO_2})Ni$^{II}_3$] exhibit reversible oxidations at 0.22 V versus Fc$^+$/Fc and 0.52 V versus Fc$^+$/Fc, respectively. The oxidized species [(talen$^{t-Bu_2}$)Ni$_3$]$^+$ and [(talen^{NO_2})Ni$_3$]$^+$ undergo a valence-tautomeric transformation involving a Ni^{III} and a phenoxyl radical species, as observed by EPR spectroscopy. Thus, these oxidized forms exhibit the phenomena of valence tautomerism and mixed valence simultaneously. The extent of delocalization of the radical species and of the Ni^{III} species is discussed.

Introduction

Metal complexes of the salen ligand H_2salen [= N,N′-bis(salicylidene)-ethylenediamine] and its derivatives have been studied for a long time in coordination chemistry.[1] Numerous investigations deal with synthetical, structural, physicochemical, and bioinorganic aspects and properties of these compounds. The ability of metal salen complexes to catalyze chemical transformations has been recognized for a variety of metal ions (e.g., Ni,[2,3] Cr,[4] Mn,[5] V,[6] and Al[7]). An important advantage of salen ligands for their use in

* To whom correspondence should be addressed. E-mail: tglaser@uni-muenster.de.

† Institut für Anorganische und Analytische Chemie, Münster.

‡ Organisch-Chemisches Institut, Münster.
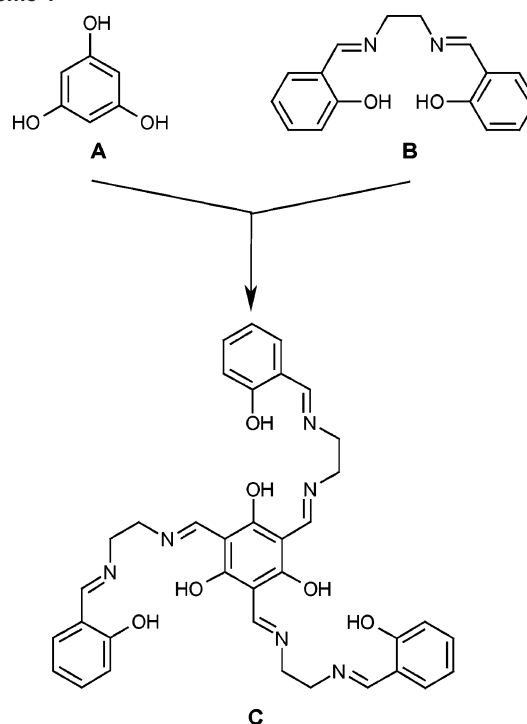
§ Max-Volmer-Laboratorium, Berlin.

∥ Max-Planck-Institut, Mülheim.

(1) (a) Pfeiffer, P.; Breith, E.; Lübbe, E.; Tsumaki, T. *Liebigs Ann. Chem.* **1933**, *503*, 84−130. (b) Pfeiffer, P.; Hesse, T.; Pfitzner, H.; Scholl, W.; Thielert, H. *J. Prakt. Chem.* **1937**, *149*, 217−296. (c) Pfeiffer, P.; Christeleit, W.; Hesse, T.; Pfitzner, H.; Thielert, H. *J. Prakt. Chem.* **1938**, *150*, 261−316. (d) Holm, R. H.; Everett, G. W.; Chakravorty, A. *Prog. Inorg. Chem.* **1966**, *7*, 83-214. (e) Calligaris, M.; Randaccio, L. In *Comprehensive Coordination Chemistry*; Wilkenson, G., Guillard, R. D., McCleverty, J. A., Eds.; Pergamon: Oxford, U. K., 1987; Vol. 2, pp 715−738.

catalysis is the opportunity for systematic variations of their steric and electronic properties.[3,5,8] The discovery by Jacobsen and co-workers and Katsuki and co-workers that chiral metal salen complexes act as effective enantioselective catalysts[9,10] led to a revival of the coordination chemistry of salen ligands. A folded geometry of the salen ligand accompanied by the formation of a chiral pocket has been argued to be an essential element for their enantioselectivity.[11–13] For the asymmetric nucleophilic ring opening of epoxides by chromium salen complexes, a mechanism was established involving catalyst activation of both the nucleophile and the electrophile in a bimetallic rate-determining step.[14] Such a cooperative reactivity between multiple metal centers is a common feature in metallo enzyme systems.[15] By using covalently linked dinuclear salen systems, not only the intramolecular pathway but also an intermolecular pathway was enhanced.[16] This observation "indicates that dimer reacts more rapidly with dimer, than does monomer with monomer" and "suggests that the design of covalently linked systems bearing three or more metal salen units may be worthwhile."[17]

We have designed a ligand **C** containing three salen units **B** covalently bridged by a common phloroglucinol (= 1,3,5-

Scheme 1

trihydroxybenzene) unit **A** in a *meta*-phenylene arrangement (Scheme 1).[18] This triple tetradentate ligand **C**, which we call triplesalen, has been designed primarily for the targeted synthesis of single-molecule magnets. These are transition-metal complexes that exhibit slow relaxation of the magnetization at low-temperatures, resulting in a hysteresis of the magnetization of a purely molecular origin.[19] The necessary requirements for the design of a single-molecule magnet are a high-spin ground state and strong magnetic anisotropy of the easy-axes type. The triplesalen ligand **C** combines the phloroglucinol bridging unit **A** for ferromagnetic couplings and, thus, high-spin ground states with the coordination environment of a salen ligand **B** for strong magnetic anisotropy. We and others have shown that the phloroglucinol bridging unit **A** acts as a ferromagnetic coupler in trinuclear transition-metal complexes by the spin-polarization mechanism. Using phloroglucinol as a bridging ligand between three (Tp*)Mo^{V}OCl fragments [Tp* = tris(3,5-dimethylpyrazolyl)hydroborate] resulted in ferromagnetic interactions between the three Mo^V centers with an $S_t = {}^3/_2$ spin ground state.[20] We have attached pendant arms at the 2,4,6 position

(2) (a) Yoon, H.; Burrows, C. J. *J. Am. Chem. Soc.* **1988**, *110*, 4087–4089. (b) Yoon, H.; Wagler, T. R.; O'Connor, K. J.; Burrows, C. J. *J. Am. Chem. Soc.* **1990**, *112*, 4568–4570.
(3) DiMauro, E. F.; Kozlowski, M. C. *Organometallics* **2002**, *21*, 1454–1461.
(4) (a) Siddall, T. L.; Miyaura, N.; Huffman, J. C.; Kochi, J. K. *J. Chem. Soc., Chem. Commun.* **1983**, 1185–1186. (b) Samsel, E. G.; Srinivasan, K.; Kochi, J. K. *J. Am. Chem. Soc.* **1985**, *107*, 7606–7617.
(5) Srinivasan, K.; Michaud, P.; Kochi, J. K. *J. Am. Chem. Soc.* **1986**, *108*, 2309–2320.
(6) Nakajima, K.; Kojima, M.; Fujita, J. *Chem. Lett.* **1986**, 1483–1486.
(7) (a) Vincens, V.; Le Borgne, A.; Spassky, N. *Makromol. Chem., Rapid Commun.* **1989**, *10*, 623. (b) Atwood, D. A.; Jegier, J. A.; Rutherford, D. *J. Am. Chem. Soc.* **1995**, *117*, 7.
(8) Srinivasan, K.; Kochi, J. K. *Inorg. Chem.* **1985**, *24*, 4671–4679.
(9) (a) Zhang, W.; Loebach, J. L.; Wilson, S. R.; Jacobsen, E. N. *J. Am. Chem. Soc.* **1990**, *112*, 2801–2803. (b) Irie, R.; Noda, K.; Ito, Y.; Matsumoto, N.; Katsuki, T. *Tetrahdron Lett.* **1990**, *31*, 7345–7348. (c) Larrow, J. F.; Jacobsen, E. N.; Gao, Y.; Hong, Y.; Nie, X.; Zepp, C. M. *J. Org. Chem.* **1994**, *59*, 1939–1942. (d) Sasaki, H.; Irie, R.; Hamada, T.; Suzuki, K.; Katsuki, T. *Tetrahedron* **1994**, *50*, 11827–11838. (e) Martínez, L. E.; Leighton, J. L.; Carsten, D. H.; Jacobsen, E. N. *J. Am. Chem. Soc.* **1995**, *117*, 5897–5898.
(10) Zhang, W.; Jacobsen, E. N. *J. Org. Chem.* **1991**, *56*, 2296–2298.
(11) (a) Hamada, T.; Fukuda, T.; Imanishi, H.; Katsuki, T. *Tetrahedron* **1996**, *52*, 515–530. (b) Ito, Y. N.; Katsuki, T. *Bull. Chem. Soc. Jpn.* **1999**, *72*, 603–619. (c) Ryan, K. M.; Bousquet, C.; Gilheany, D. G. *Tetrahdron Lett.* **1999**, *40*, 3613–3616. (d) Jacobsen, H.; Cavallo, L. *Chem.—Eur. J.* **2001**, *7*, 800–807. (e) El-Bahraoui, J.; Wiest, O.; Feichtinger, D.; Plattner, D. A. *Angew. Chem., Int. Ed.* **2001**, *40*, 2073–2076. (f) Cavallo, L.; Jacobsen, H. *J. Org. Chem.* **2003**, *68*, 6202–6207. (e) Darensbourg, D. J.; Mackiewicz, R. M.; Rodgers, J. L.; Fang, C. C.; Billodeaux, D. R. *Inorg. Chem.* **2004**, *43*, 6024–6034.
(12) Cavallo, L.; Jacobsen, H. *Eur. J. Inorg. Chem.* **2003**, 892–902.
(13) Bandini, M.; Cozzi, P. G.; Umanchi-Ronchi, A. *J. Chem. Soc., Chem. Commun.* **2002**, 919–927.
(14) (a) Hansen, K. B.; Leighton, J. L.; Jacobsen, E. N. *J. Am. Chem. Soc.* **1996**, *118*, 10924–10925. (b) Darensbourg, D. J.; Yarbrough, J. C. *J. Am. Chem. Soc.* **2002**, *124*, 6335–6342. (c) Darensbourg, D. J.; Mackiewicz, R. M.; Phelps, A. L.; Billodeaux, D. R. *Acc. Chem. Res.* **2004**, *37*, 836–844.
(15) (a) Sträter, N.; Lipscomb, W. N.; Klabunde, T.; Krebs, B. *Angew. Chem., Int. Ed. Engl.* **1996**, *35*, 2024–2055. (b) Averill, B. A. In *Comprehensive Coordination Chemistry II*; McCleverty, J. A., Meyer, T. J., Eds.; Elsevier Ltd.: Oxford, U. K., 2004; Vol. 8, pp 641–676.
(16) Konsler, R. G.; Karl, J.; Jacobsen, E. N. *J. Am. Chem. Soc.* **1998**, *120*, 10780–10781.
(17) Jacobsen, E. N. *Acc. Chem. Res.* **2000**, *33*, 421–431.
(18) Glaser, T.; Heidemeier, M.; Lügger, T. *J. Chem. Soc., Dalton Trans.* **2003**, 2381–2383.
(19) (a) Long, J. R. In *Chemistry of Nanostructured Materials*; Yang, P., Ed.; World Scientific: Hong Kong, 2003; pp 291–315. (b) Sessoli, R.; Gatteschi, D.; Caneschi, A.; Novak, M. A. *Nature* **1993**, *365*, 141–143. (c) Sessoli, R.; Tsai, H. L.; Schake, A. R.; Wang, S. Y.; Vincent, J. B.; Folting, K.; Gatteschi, D.; Christou, G.; Hendrickson, D. N. *J. Am. Chem. Soc.* **1993**, *115*, 1804–1816. (d) Gatteschi, D.; Caneschi, A.; Pardi, L.; Sessoli, R. *Science* **1994**, *265*, 1054–1058. (e) Gatteschi, D.; Sessoli, R. *Angew. Chem., Int. Ed.* **2003**, *42*, 268–297. (f) Gatteschi, D.; Sorace, L. *J. Solid State Chem.* **2001**, *159*, 253–261. (g) Delfs, C.; Gatteschi, D.; Pardi, L.; Sessoli, R.; Wieghardt, K.; Hanke, D. *Inorg. Chem.* **1993**, *32*, 3099–3103.
(20) Ung, V. A.; Thompson, A.; Bardwell, D. A.; Gatteschi, D.; Jeffery, J. C.; McCleverty, J. A.; Totti, F.; Ward, M. D. *Inorg. Chem.* **1997**, *36*, 3447–3454.

of phloroglucinol in order to enhance the stability of first-row transition-metal complexes by the chelate effect.[21] This concept has been successfully applied to obtain ferromagnetic interactions between three Cu^{II} ions through the spin-polarization mechanism with $S_t = {}^3/_2$ spin ground states.[21,22] To introduce magnetic anisotropy, we have been choosing a salen-like coordination environment, which is known to establish a pronounced magnetic anisotropy by its strong ligand field in the basal plane.[23,24] A well-studied example is the Jacobsen catalyst [(salen′)Mn^{III}Cl] [H_2salen′ = (R,R)-*N*,*N*′-bis(3,5-di-*tert*-butylsalicylidene)-1,2-cyclohexanedi-amine],[10] which is a Mn^{III} (S = 2) species with a zero-field splitting of $D = -2.5$ cm^{-1}.[23,25]

In a recent communication, we described the successful synthesis of the first triplesalen ligand H_6talen {= 2,4,6-tris[1-(2-salicylaldimino-2-methyl-propylimino)-ethyl]-1,3,5-trihydroxybenzene} and the structure of its trinuclear Ni^{II} complex [(talen)Ni$^{II}_3$].[18] The analogous trinuclear Cu^{II} complex [(talen)Cu$^{II}_3$] exhibits ferromagnetic couplings between the three local $S = {}^1/_2$ spins, resulting in an $S_t = {}^3/_2$ spin ground state.[26] EPR spectra display a 10-line hyperfine splitting pattern due to the coupling of the total electron spin with the individual Cu nuclear spins ($I = 3/2$) according to the rule $2 \times n \times I + 1$. Density functional calculations demonstrate that the spin-density on adjacent carbon atoms of the central benzene rings alters in the quartet ground state in accordance with the spin-polarization mechanism.[26]

In this paper, we present a detailed study of the electronic and steric effects caused by changing the substituents at the terminal phenolates of the triplesalen ligand. These substitution-dependent effects on the geometric and electronic structure of the trinuclear nickel complexes are examined by single-crystal X-ray diffraction studies, FTIR and resonance Raman (rR) studies, electronic absorption spectroscopy, and electrochemical investigations. Additionally, electrochemically generated oxidized species are investigated by spectroelectrochemistry and EPR spectroscopy to elucidate the electronic structure of these oxidized species with regard to their Ni^{III} or radical character and to the delocalization respective communication between the three metal—salen subunits. This study builds the base for the use of these trinuclear nickel complexes as homogeneous catalysts in alkene epoxidation. In mononuclear nickel salen catalysts, the importance of a high-valent nickel—oxygen species has been identified.[2] Additionally, this detailed study on the properties of a series of triplesalen ligands and their Ni complexes builds the base for our ongoing studies involving

other metal ions to rationally develop new types of single-molecule magnets.

Experimental Section

Preparations of Compounds. 2,4,6-Tris[1-(2-amino-2-methyl-propylimino)-ethyl]-1,3,5-trihydroxybenzene, H_6talen {= 2,4,6-tris-[1-(2-salicylaldimino-2-methyl-propylimino)-ethyl]-1,3,5-trihydroxy-benzene}, and [(talen)Ni$_3$] were synthesized as described previously.[18]

2,4,6-Tris{1-[2-(3,5-di-*tert*-butylsalicylaldimino)-2-methylpro-pylimino]-ethyl}-1,3,5-trihydroxybenzene (H_6talen$^{t-Bu_2}$). 2,4,6-Tris[1-(2-amino-2-methylpropylimino)-ethyl]-1,3,5-trihydroxybenzene (1.00 g, 2.16 mmol) and 3,5-di-*tert*-butyl-2-hydroxybenzaldehyde (1.52 g, 6.49 mmol) were stirred in EtOH (15 mL) for 16 h, during which a yellow precipitate formed. This was filtered off, washed with a minimum amount of EtOH, and dried under a high vacuum. Yield: 1.61 g (67%). ^{1}H NMR (400.14 MHz, CDCl$_3$): $\delta = 1.28$ [s, 18H; C(CH$_3$)$_2$], 1.31 [s, 27H; C(CH$_3$)$_3$], 1.45 [s, 27H; C(CH$_3$)$_3$], 2.47 (m, 9H; CH$_3$), 3.51 (m, 6H; CH$_2$), 7.10 (s, 3H; C4), 7.39 (s, 3H; C6), 8.38 (m, 3H; N=C−H), 13.4−15.3 (m, 6H; OH). ^{13}C NMR (50.33 MHz, CDCl$_3$): $\delta = 18.4$ (N=C−CH_3); 25.1 [br, C(CH_3)$_2$]; 29.4 [C(CH_3)$_3$]; 31.5 [C(CH_3)$_3$]; 34.1 [C(CH$_3$)$_3$]; 35.0 [C(CH$_3$)$_3$]; 54.2 (CH$_2$); 59.8 [C(CH$_3$)$_2$]; 163.2 (N=C−H); 170.5, 170.7, 171.2 (all N=C−CH$_3$); central benzene ring 105.1, 105.9, 107.0, 108.6 (all C−C=N); 185.6 (br, C−OH); terminal benzene rings 117.8 (C1), 126.3 and 126.9 (C4 and C6), 136.6 and 139.9 (C3 and C5), 163.2 (C2). MS−MALDI−TOF *m/z*: 1112.0 [M + H]$^+$, 1134.0 [M + Na]$^+$. IR (KBr): $\tilde{\nu}$/cm^{-1} = 3048w, 2961s, 2909m, 2869m, 2800br, 1628s, 1537vs, 1457s, 1442s, 1389m, 1362m, 1372m, 1327m, 1274w, 1252w, 1166m, 1132w, 878w, 829w, 773w. Anal. Calcd for C$_{69}$H$_{104}$N$_6$O$_7$: C, 73.37; H, 9.28; N, 7.44. Found: C, 73.68; H, 9.00; N, 7.35.

2,4,6-Tris{1-[2-(5-nitrosalicylaldimino)-2-methylpropylimino]-ethyl}-1,3,5-trihydroxybenzene (H_6talen^{NO_2}). 2,4,6-Tris[1-(2-amino-2-methylpropylimino)-ethyl]-1,3,5-trihydroxybenzene (500 mg, 1.08 mmol) and 5-nitro-2-hydroxybenzaldehyde (542 mg, 3.24 mmol) were stirred in EtOH (20 mL) for 16 h, during which an orange precipitate formed. This was filtered off, washed with a minimum amount of EtOH, and dried in a vacuum. Yield: 840 mg (85%). ^{1}H NMR (598.97 MHz, d$_7$-DMF): $\delta = 1.52$ [s, 18H; C(CH$_3$)$_2$], 2.44 (s, 9H; CH$_3$), 3.76 (m, 6H; CH$_2$), 6.88 [d, ^3J(H,H) = 9.4 Hz, 3H; C6], 8.16 [dd, ^3J(H,H) = 9.4, ^4J(H,H) = 3.0 Hz, 3H; C4], 8.54 (s, br, 3H; C3), 8.93 (s, br, 3H; N=C−H), 13−15 (m, 6H; OH). ^{13}C NMR (150.63 MHz, d$_7$-DMF): $\delta = 18.4$ (N=C−CH_3); 24.6 [C(CH_3)$_2$]; 53.6 (CH$_2$); 60.8 [C(CH$_3$)$_2$]; 164.6 [N=C−H]; 172.6 (N=C−CH$_3$); central benzene ring 106.0 (br, C−C=N), 185.9 (C−OH); terminal benzene rings 117.0 (C1), 120.6 (C3), 129.0 (C4), 130.8 (C6), 137.9 (C5), 172.2 (C2). MS−MALDI−TOF *m/z*: 907.6 [M − H]$^-$. IR (KBr): $\tilde{\nu}$/cm^{-1} = 3065w, 3000 br, 2975w, 2931w, 2872w, 1633s, 1618s, 1537vs, 1459s, 1442s, 1392m, 1373m, 1337vs, 1297m, 1236w, 1129m, 1094w, 834w, 754w. Anal. Calcd for C$_{45}$H$_{53}$N$_9$O$_{13}$: C, 58.24; H, 5.76; N, 13.58. Found: C, 58.15; H, 5.37; N, 13.45.

[(talen$^{t-Bu_2}$)Ni$_3$]. A solution of H_6talen$^{t-Bu_2}$ (200 mg, 0.180 mmol) in EtOH (15 mL) was added dropwise to a solution of Ni-(OAc)$_2$·4H$_2$O (134 mg, 0.540 mmol) in EtOH (15 mL). The resulting red suspension was heated to reflux for 1 h. The orange-red, microcrystalline precipitate was filtered off, washed with diethyl ether, and dried in a vacuum. Yield: 197 mg (85%). ^{1}H NMR (400.14 MHz, CDCl$_3$): $\delta = 1.25$ [s, 27H; C(CH$_3$)$_3$], 1.32 [s, 27H; C(CH$_3$)$_3$], 1.34 [s, 18H; C(CH$_3$)$_2$], 2.36 (s, 9H; CH$_3$), 3.18 (s, 6H; CH$_2$), 6.85 [d, ^4J(H,H) = 2.5 Hz, 3H; C4], 7.22 [d, ^4J(H,H) = 2.5

(21) Glaser, T.; Gerenkamp, M.; Fröhlich, R. *Angew. Chem., Int. Ed.* **2002**, *41*, 3823−3825.
(22) Glaser, T.; Heidemeier, M. Unpublished results.
(23) Kennedy, B. J.; Murray, K. S. *Inorg. Chem.* **1985**, *24*, 1552−1557.
(24) (a) Mitra, S. *Prog. Inorg. Chem.* **1977**, *22*, 309−408. (b) Bencini, A.; Ciofini, I.; Uytterhoeven, M. G. *Inorg. Chim. Acta* **1998**, *274*, 90−101.
(25) (a) Campbell, K. A.; Lashley, M. R.; Wyatt, J. K.; Nantz, M. H.; Britt, R. D. *J. Am. Chem. Soc.* **2001**, *123*, 5710−5719. (b) Krzystek, J.; Telser, J. *J. Magn. Reson.* **2003**, *162*, 454−465.
(26) Glaser, T.; Heidemeier, M.; Grimme, S.; Bill, E. *Inorg. Chem.* **2004**, *43*, 5192−5194.

Hz, 3H; C6], 7.38 (s, 3H; N=C−H). ^{13}C NMR (100.63 MHz, CDCl$_3$): δ = 23.1 (CH$_3$); 26.3 [C(*C*H$_3$)$_3$]; 29.7 [C(*C*H$_3$)$_3$]; 31.3 [*C*(CH$_3$)$_3$]; 33.8 [*C*(CH$_3$)$_3$]; 35.5 [*C*(CH$_3$)$_3$]; 66.0 [*C*(CH$_3$)$_2$]; 65.5 (CH$_2$); 158.6 (N=*C*−H); 170.0 (N=*C*−CH$_3$); central benzene ring 110.6 (*C*−C=N), 170.8 (*C*−OH); terminal benzene rings 119.9 (C1), 126.1 (C4), 128.5 (C6), 135.5 and 139.3 (C3 and C5), 161.8 (C2). MS−MALDI−TOF *m/z*: 1280.5 [M]$^+$. IR (KBr): $\tilde{\nu}$/cm^{-1} = 3037w, 2959s, 2905m, 2867m, 1615s, 1562s, 1531m, 1479vs, 1437s, 1388m, 1361w, 1339w, 1300s, 1276w, 1257m, 1190m, 1173s, 1070w, 845w, 786w, 584w. Anal. Calcd for C$_{69}$H$_{96}$N$_6$O$_6$-Ni$_3$: C, 64.66; H, 7.55; N, 6.50. Found: C, 64.22; H, 7.46; N, 6.25.

[(talen^{NO_2})Ni$_3$]. A solution of H$_6$talen^{NO_2} (200 mg, 0.220 mmol) in DMF (4 mL) was added dropwise to a solution of Ni(OAc)$_2$·4H$_2$O (169 mg, 0.680 mmol) in DMF (4 mL). The resulting red suspension was heated to reflux for 2 h. The orange-red, micro-crystalline precipitate was filtered off, washed with diethyl ether, and dried in a vacuum. Yield: 157 mg (66%). MS−MALDI−TOF *m/z*: 1078.5 [M]$^+$. IR (KBr): $\tilde{\nu}$/cm^{-1} = 3064w, 2969w, 2922w, 2862w, 1606s, 1550s, 1472vs, 1389m, 1322vs, 1299s, 1245w, 1194m, 1099m, 950w, 834w, 673w, 651. Anal. Calcd for C$_{45}$H$_{47}$N$_9$O$_{13}$Ni$_3$: C, 49.23; H, 4.31; N, 11.48. Found: C, 49.17; H, 4.03; N, 11.51.

X-ray Crystallography. The data set for [(talen$^{t-Bu_2}$)Ni$^{II}_3$] was collected on a Bruker AXS APEX diffractometer, and the one for [(talen^{NO_2})Ni$^{II}_3$] was collected with a Nonius KappaCCD diffractometer; both were equipped with rotating anode generators. Programs used: data collection, [(talen$^{t-Bu_2}$)Ni$^{II}_3$] SMART[27] and [(talen^{NO_2})Ni$^{II}_3$] COLLECT;[28] data reduction, [(talen$^{t-Bu_2}$)Ni$^{II}_3$] SMART[27] and [(talen^{NO_2})Ni$^{II}_3$] Denzo-SMN;[29] absorption correction for [(talen^{NO_2})Ni$^{II}_3$], SORTAV;[30] structure solution, SHELXS-97;[31] structure refinement, SHELXL-97;[32] graphics, Diamond.[33]

Analysis of [(talen$^{t-Bu_2}$)Ni$^{II}_3$]: formula C$_{69}$H$_{96}$N$_6$Ni$_3$O$_6$, M = 1281.65, red crystal 0.12 × 0.08 × 0.02 mm, a = 19.6170(8) Å, c = 23.2168(14) Å, γ = 120°, V = 7737.5(6) Å^3, ρ_{calc} = 1.100 g cm^{-3}, μ = 7.69 cm^{-1}, no absorption correction (0.913 ≤ T ≤ 0.985), Z = 4, trigonal, space group $P\bar{3}c1$ (No. 165), λ = 0.710 73 Å, T = 173 K, ω and φ scans, 59 630 reflections collected (±h, ±k, ±l), [(sinθ)/λ] = 0.60 Å^{-1}, 4578 independent (R_{int} = 0.075) and 3164 observed reflections [$I \geq 2 \sigma(I)$], 262 refined parameters, R = 0.037, wR_2 = 0.107, max. residual electron density = 0.93 (−0.23) e Å^{-3}, hydrogen atoms calculated and refined riding.

Analysis of [(talen^{NO_2})Ni$^{II}_3$]: formula C$_{45}$H$_{45}$N$_9$Ni$_3$O$_{12}$·3C$_3$H$_7$-NO, M = 1299.32, red crystal 0.50 × 0.25 × 0.05 mm, a = 14.489-(1) Å, b = 14.606(1) Å, c = 15.744(1) Å, α = 112.06(1)°, β = 109.85(1)°, γ = 91.59(1)°, V = 2858.0(5) Å^3, ρ_{calc} = 1.510 g cm^{-3}, μ = 10.56 cm^{-1}, empirical absorption correction (0.620 ≤ T ≤ 0.949), Z = 2, triclinic, space group $P\bar{1}$ (No. 2), λ = 0.710 73 Å, T = 198 K, ω and φ scans, 30 042 reflections collected (±h, ±k, ±l), [(sinθ)/λ] = 0.59 Å^{-1}, 9989 independent (R_{int} = 0.053) and 7214 observed reflections [$I \geq 2 \sigma(I)$], 697 refined parameters, R = 0.068, wR_2 = 0.205. The three solvent molecules show severe disorder and were treated with isotropic thermal parameters; a refinement with split positions did not improve the model. Max.

residual electron density = 1.30 (−0.90) e Å^{-3} close to the solvent molecules, hydrogen atoms calculated and refined riding.

Other Physical Measurements. Infrared spectra (400−4000 cm^{-1}) of solid samples were recorded on a Bruker Vector 22 spectrometer as KBr disks. UV−vis−NIR absorption spectra of the solutions were measured on a Varian Cary 50 spectrophotometer in the range 190−1100 nm at ambient temperatures. ESI and MALDI−TOF mass spectra were recorded on a Micromass Quattro LC mass spectrometer and a Bruker Reflex IV mass spectrometer, respectively. ^{1}H and ^{13}C NMR spectra were measured on a Bruker AC200 spectrometer, a Bruker AMX400, or a Varian Unity plus 600 spectrometer using the solvent as an internal standard. The electrochemical experiments were performed on Ar-flushed CH$_2$-Cl$_2$ solutions containing 0.2 M [NBu$_4$]PF$_6$ in a classical three-electrode cell. The working electrode was a glassy carbon disk electrode, the counter electrode a platinum wire, and the reference electrode was Ag/0.01 M AgNO$_3$/CH$_3$CN. All potentials are referenced to the ferrocenium/ferrocene (Fc$^+$/Fc) couple used as an internal standard. The electrochemical cell was connected to a EG&G potentiostat/galvanostat model 273A. EPR spectra of frozen solutions and powdered solids were recorded on a Bruker ESP 200E spectrometer equipped with a helium flow cryostat (X-band Oxford Instruments ESR 910). The X-band resonator was a standard rectangular cavity ER4102. rR spectra were recorded with a double monochromator (Spex 1403, 2400/mm holographic gratings) equipped with a photomultiplier using the 413 nm line of a krypton ion laser. The spectral bandwidth was 2.8 cm^{-1} and the wavenumber increment 1 cm^{-1}.

Results and Analysis

Synthesis and Characterization. The preparation of symmetrical salen-type ligands is routinely achieved by the Schiff-base condensation of ethylenediamine or another diamine with two equivalents of an aldehyde or ketone. However, the targeted triplesalen ligand contains three unsymmetrically substituted ethylenediamine units (Scheme 1). The controlled synthesis of unsymmetrical salen-type ligands (not statistical mixtures of unsymmetrical and symmetrical compounds) containing two different phenol derivatives is not trivial[34] and affords, in a first step, the isolation of a monocondensed diamine derivative, a so-called *salen half unit*.[35] In this respect, two principle reaction routes are feasible for the preparation of the targeted triplesalen ligand **C** (Scheme 2). Route A requires the synthesis of a salen half unit **E** in the first step, which reacts in the second step with a triscarbonyl derivative of phloroglucinol **D**. Route B requires the synthesis of a half unit of the triplesalen ligand **G,** which reacts in the second step with an *ortho*-carbonyl derivative of phenol **F**.

The half unit **E** of neither the parent H$_2$salen nor its ketimine derivative H$_2$Me$_2$salen {= N,N′-bis[1-(2-hydroxy-phenyl)-ethylidene]-ethylenediamine} is accessible.[34] The reaction of salicylaldehyde with a 100-fold excess of ethylenediamine at low temperatures yields only symmetric

(27) *SMART*; Bruker AXS: Madison, Wisconsin, 2000.
(28) *COLLECT*; Nonius B. V.: Delft, The Netherlands, 1998.
(29) Otwinowski, Z.; Minor, W. *Methods Enzymol.* **1997**, *276*, 307−326.
(30) (a) Blessing, R. H. *Acta Crystallogr., Sect. A* **1995**, *A51*, 33−37. (b) Blessing, R. H. *J. Appl. Crystallogr.* **1997**, *30*, 421−426.
(31) Sheldrick, G. M. *Acta Crystallogr., Sect. A* **1990**, *A46*, 467−473.
(32) Sheldrick, G. M. *SHELXL-97*; Universität Göttingen: Göttingen, Germany, 1997.
(33) Brandenburg, K. *DIAMOND*; Universität Bonn: Bonn, Germany, 1997.

(34) Hernández-Molina, R.; Mederos, A. In *Comprehensive Coordination Chemistry II*; McCleverty, J. A., Meyer, T. J., Eds.; Elsevier Ltd.: Oxford, U. K., 2004; Vol. 1, pp 411−446.
(35) (a) Lopez, J.; Liang, S.; Bu, X. R. *Tetrahedron Lett.* **1998**, *39*, 4199−4202. (b) Janssen, K. B. M.; Laquierra, I.; Dehaen, W.; Parton, R. F.; Vankelecom, I. F. J.; Jacobs, P. A. *Tetrahedron: Asymmetry* **1997**, *8*, 3481−3487.

Scheme 2
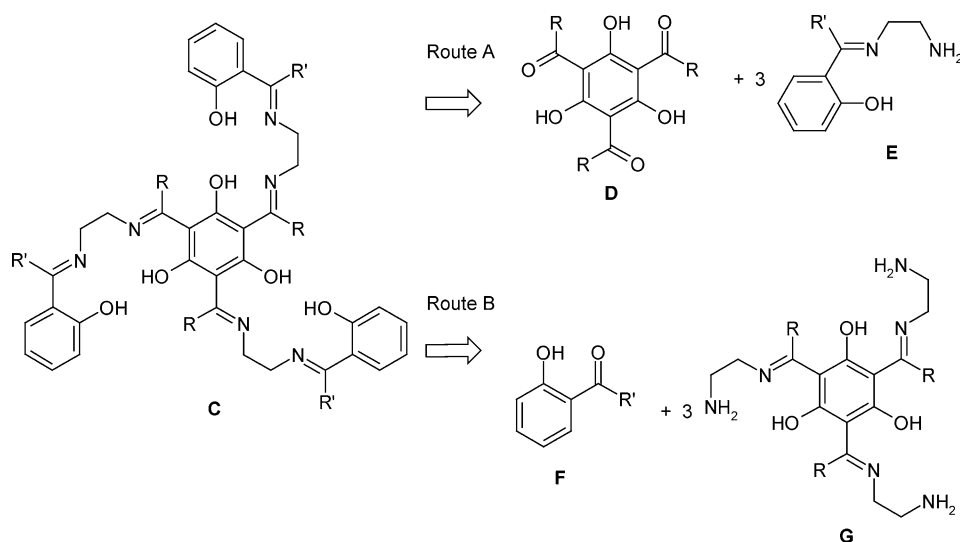
H$_2$salen. Thus, the key step in the synthesis of a triplesalen ligand **C** is the preparation of a half unit, either **E** or **G**. Several methods for the preparation and isolation of derivatives of the parent salen half unit are described in the literature.[16,35,36,37] We applied several of these methods for the synthesis of a triplesalen ligand and obtained a variety of unexpected new compounds.[22] The successful synthesis of the triplesalen ligand is based on the observation of Elias and co-workers that the asymmetric diamine 1,2-diamino-2-methylpropane reacts with 2-hydroxyacetophenone by a regioselective attack of the sterically less shielded amino group in the 1 position at the carbonyl function of the ketone to give a derivative of the salen half unit **E**.[37] The remaining sterically more shielded amino group of this salen half unit reacts with salicylaldehyde to form an unsymmetrical salen derivative with one ketimine and one aldimine function.[37] To apply this strategy to the preparation of a triplesalen ligand, we chose route B (Scheme 2) starting from the triketone **1** of phloroglucinol (Scheme 3). The reaction of **1** with excess 1,2-diamino-2-methylpropane (using the diamine as a solvent) regioselectively yielded the triplesalen half unit **2**.[18] Only the sterically less hindered amino group reacted with the carbonyl functions of the triketone **1**.

The triplesalen ligand H$_6$talen was synthesized by reacting the triplesalen half unit **2** with salicylaldehyde using the aldehyde as a solvent.[18] This protocol is not applicable for the use of 3,5-di-*tert*-butyl-2-hydroxybenzaldehyde and 5-nitro-2-hydroxybenzaldehyde, which are solids. Thus, the condensation of these two aldehydes with the triplesalen half unit **2** has been performed in a minimum amount of EtOH, yielding the triplesalen ligands H$_6$talen$^{t-Bu_2}$ and H$_6$talen^{NO_2} in good yields as yellow and orange solids, respectively. The identity and purity of these ligands have been confirmed by

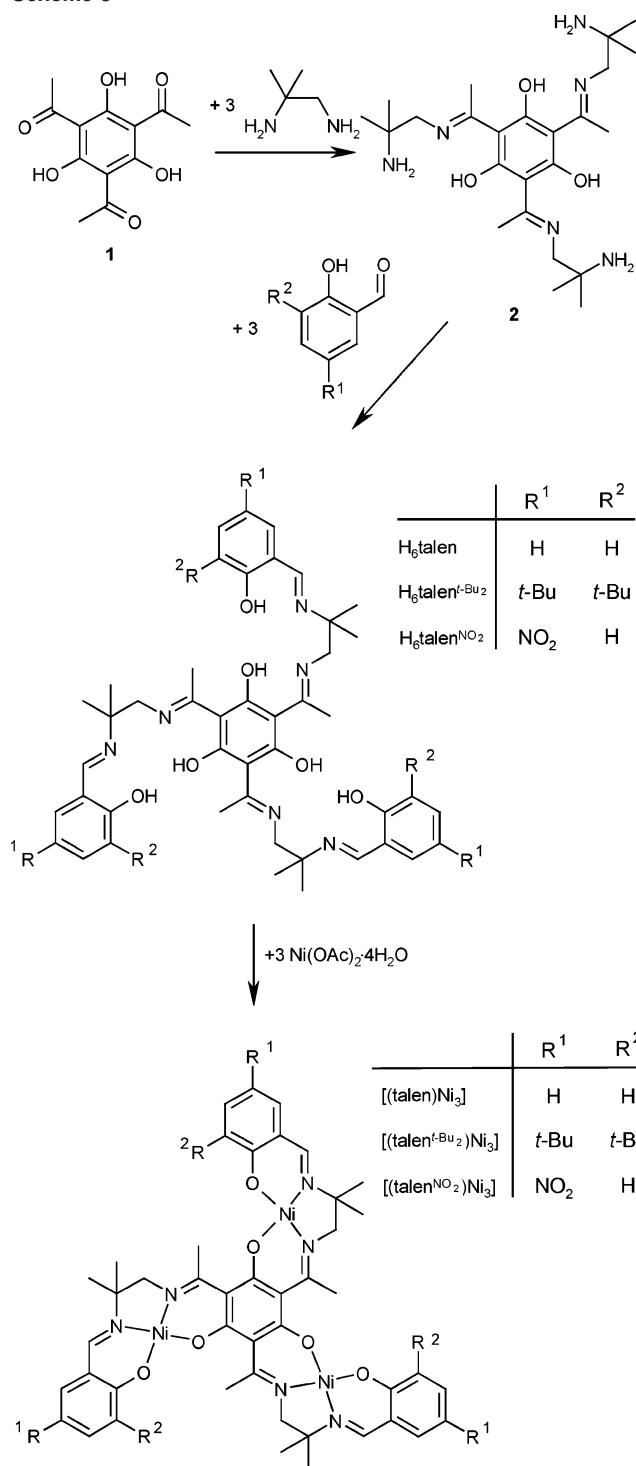mass spectrometry, FTIR, elemental analysis, and NMR spectroscopy.

The reaction of the ligands H$_6$talen and H$_6$talen$^{t-Bu_2}$ with nickel acetate in EtOH afforded [(talen)Ni$^{II}_3$] and [(talen$^{t-Bu_2}$)-Ni$^{II}_3$], respectively, as orange-red microcrystalline solids, whereas the reaction of H$_6$talen^{NO_2} with nickel acetate had to be performed in DMF because of the poor solubility of H$_6$talen^{NO_2} in all other solvents, resulting in microcrystalline red [(talen^{NO_2})Ni$^{II}_3$] (Scheme 3). The successful synthesis of the three trinuclear complexes was confirmed by mass spectrometry, FTIR, and elemental analysis. Whereas [(talen)Ni$^{II}_3$] and [(talen$^{t-Bu_2}$)Ni$^{II}_3$] are soluble in organic solvents such as CH$_2$Cl$_2$, CHCl$_3$, CH$_3$CN, or toluene, [(talen^{NO_2})Ni$^{II}_3$] is only sparingly soluble in DMF. Thus, only [(talen)Ni$^{II}_3$] and [(talen$^{t-Bu_2}$)Ni$^{II}_3$] have been characterized by ^{1}H and ^{13}C NMR spectroscopy in solution. The spectra are consistent with C_{3h} symmetry for the trinuclear complexes exhibiting only one singlet for the two methyl groups of the diimine units. This is in contrast with the solid-state structures (vide infra), where the methyl groups of each dimethyl unit are discriminated: one methyl group lies in the plane of the salen subunit (equatorial methyl group), whereas the other is directed perpendicular to the salen subunit (axial methyl group). Thus, the interconversion between λ and δ configurations of the five-membered chelate rings Ni−N−C−C−N is fast on the NMR time scale.

Crystal and Molecular Structures. The crystal structures of complexes [(talen)Ni$^{II}_3$]·CHCl$_3$·0.5toluene,[18] [(talen$^{t-Bu_2}$)-Ni$^{II}_3$], and [(talen^{NO_2})Ni$^{II}_3$]·3DMF were determined by single-crystal X-ray diffraction at 153, 173, and 198 K, respectively. Each structure contains neutral trinuclear complexes in which one 6-fold-deprotonated triplesalen ligand (talen^X)$^{6-}$ coordinates three Ni^{II} ions. The molecular structures of [(talen$^{t-Bu_2}$)-Ni$^{II}_3$] and [(talen^{NO_2})Ni$^{II}_3$] are both displayed in Figure 1, and selected interatomic distances and angles are summarized in Table S1 (Supporting Information). The corresponding values for [(talen)Ni$^{II}_3$]·CHCl$_3$·0.5toluene[18] are included for comparison. The Ni^{II} ions are four-coordinated in a square-planar coordination environment of two phenolate and two

(36) (a) Atkins, R.; Brewer, G.; Kokot, E.; Mockler, G. M.; Sinn, E. *Inorg. Chem.* **1985**, *24*, 127−134. (b) Fernandey Garcia, M. I.; Fondo, M.; Garcia Deibe, A. M.; Fernandez Fernandez, M. B.; Gonzalez, A. M. *Z. Anorg. Allg. Chem.* **2000**, *626*, 1985−1991. (c) Costes, J.-P.; Dahan, F.; Dupuis, A.; Laurant, J.-P. *J. Chem. Soc., Dalton Trans.* **1998**, 1307−1314.

(37) Böttcher, A.; Elias, H.; Eisenmann, B.; Hilms, E.; Huer, A.; Kniep, R.; Röhr, C. *Z. Naturforsch., B: Chem. Sci.* **1994**, *49*, 1089−1100.

Scheme 3

	R¹	R²
H₆talen	H	H
H₆talen^{t-Bu2}	t-Bu	t-Bu
H₆talen^{NO2}	NO₂	H

+3 Ni(OAc)₂·4H₂O

	R¹	R²
[(talen)Ni₃]	H	H
[(talen^{t-Bu2})Ni₃]	t-Bu	t-Bu
[(talen^{NO2})Ni₃]	NO₂	H

imine nitrogen donor atoms. Whereas [(talen^{t−Bu2})Ni^{II}₃] possesses crystallographic C_3 symmetry, [(talen)Ni^{II}₃][18] and [(talen^{NO2})Ni^{II}₃] exhibit no crystallographically imposed symmetry.

In [(talen)Ni^{II}₃], the Ni−O bond distances differ between the central and terminal phenolates. Whereas, the average Ni−O bond distance of the central phenolate is 1.82 Å, it is 1.86 Å for the terminal phenolates. This difference averages in the *tert*-butyl derivative [(talen^{t−Bu2})Ni^{II}₃] to 1.84 Å for both, the terminal and the central Ni−O phenolate bonds.

a)

b)
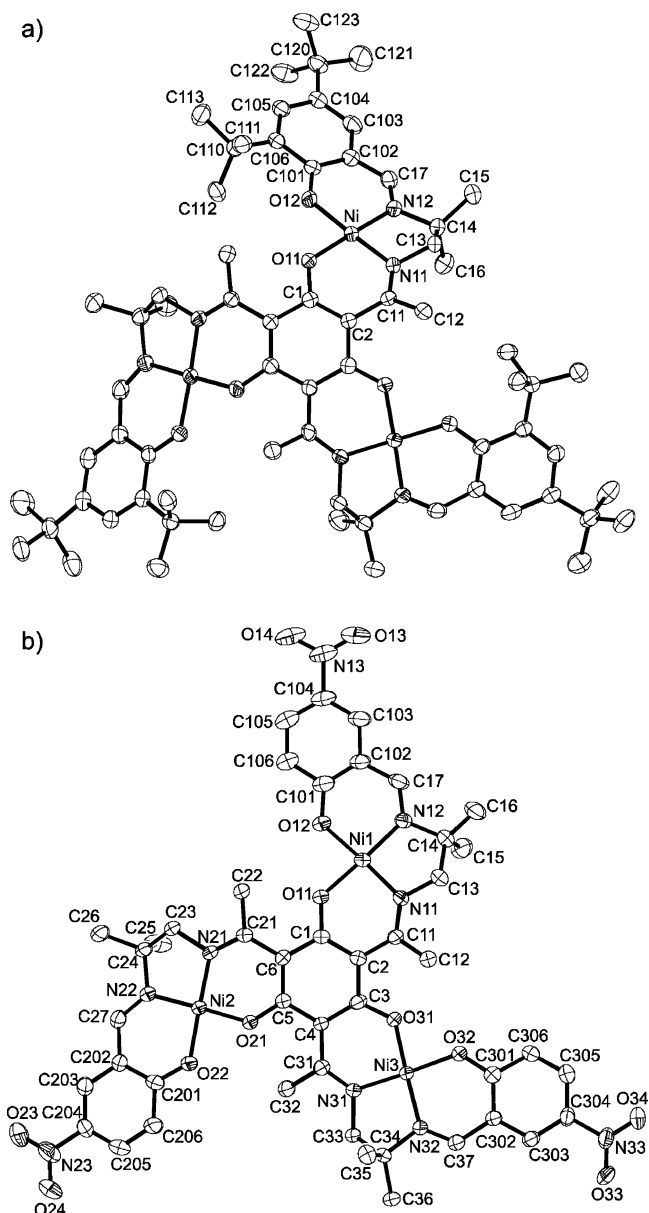
Figure 1. Molecular structures of the neutral trimers in crystals of (a) [(talen^{t−Bu2})Ni^{II}₃] and (b) [(talen^{NO2})Ni^{II}₃]·3DMF; thermal ellipsoids are drawn at the 50% probability level; hydrogen atoms are omitted for clarity.

In [(talen^{NO2})Ni^{II}₃], the mean values are 1.82 and 1.85 Å for the central and terminal Ni−O phenolate bonds, respectively.

Some mononuclear nickel salen complexes exhibit relatively strong intermolecular interactions in their crystal structures. The parent complex [(salen)Ni] is best described as a dimer {[(salen)Ni]}₂.[38] No significant intermolecular contacts occur in the trinuclear triplesalen complexes. However, there are some close contacts in the crystal structure of [(talen)Ni^{II}₃], with the shortest being an intermolecular C−C distance of 3.05 Å between two phenyl rings and an intermolecular Ni−C contact at 3.12 Å.

An important feature of the overall geometry of these trinuclear molecules is that they are not flat but bowl-shaped

(38) (a) Shkol′nikova, L. M.; Yumal, E. M.; Shugarn, E. A. *Zh. Strukt. Khim.* **1970**, *11*, 886. (b) Manfredotti, A. G.; Guastini, C. *Acta Crystallogr., Sect. C* **1983**, *39*, 863.

a)

b)

c)
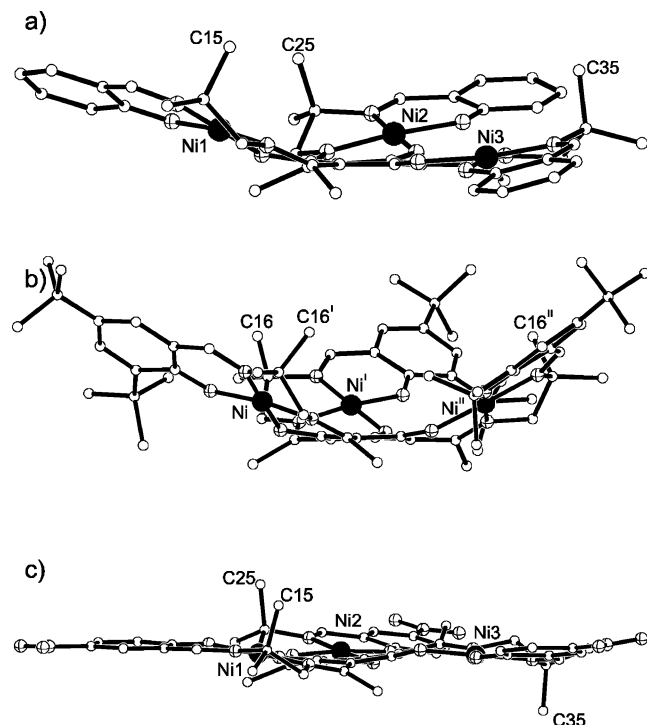
Figure 2. Molecular structures of (a) [(talen)Ni$^{II}_3$],[18] (b) [(talen$^{t-Bu_2}$)Ni$^{II}_3$], and (c) [(talen^{NO_2})Ni$^{II}_3$] drawn perpendicular to the central benzene ring of the phloroglucinol backbone.

(Figure 2). A qualitative estimate by an inspection of Figure 2 gives the following order of increasing distortion from planarity: [(talen^{NO_2})Ni$^{II}_3$] < [(talen)Ni$^{II}_3$] < [(talen$^{t-Bu_2}$)Ni$^{II}_3$]. Several geometric parameters allow for a quantitative description of this distortion. A simple measure is provided by the shortest distance d of the nickel ions from the best plane formed by the six carbon atoms of the central benzene ring of the phloroglucinol backbone (Table 1). In [(talen)-Ni$_3$], these values show a wide distribution with a mean value of 0.60 Å. The qualitative estimate of a stronger distortion in [(talen$^{t-Bu_2}$)Ni$_3$] is corroborated by $d = 1.04$ Å (no distribution due to the C_3 axes), whereas the qualitatively small distortion in [(talen^{NO_2})Ni$_3$] is corroborated by a value of 0.29 Å (the negative value for Ni3 in Table 1 corresponds to a displacement to the other side of the central plane). Although these values provide a quantitative measure for deviations from planarity, they give no geometrical information for the influence on Ni−O bonding interactions. The Ni−O bonding interactions seem to be of principle interest in the trinuclear triplesalen complexes not only for understanding the electron density at the metal ions[39] (catalytic activity) but also for the electronic communication between the three metal−salen subunits through the bridging phloroglucinol backbone (magnetic properties). Additionally, the occurrence of folding in salen complexes has been recognized to be essential for enantioselectivity in catalytic transformations.[11,12]

The mononuclear complexes of salen-type ligands exhibit several forms of distortion from planarity:[38,40−43] V-shaped distortions, helical distortions of the benzene rings relative

(39) Ottenwaelder, X.; Ruiz-Garcia, R.; Blondin, G.; Carasco, R.; Cano, J.; Lexa, D.; Journaux, Y.; Aukauloo, A. *J. Chem. Soc., Chem. Commun.* **2004**, 504−505.

Table 1. Selected Structural Properties of the Nickel Triplesalen Complexes

		[(talen)Ni$_3$]	[(talen$^{t-Bu_2}$)Ni$_3$]	[(talen^{NO_2})Ni$_3$]
d^a/Å	Ni1	0.87	1.04	0.52
	Ni2	0.69		0.20
	Ni3	0.23		−0.16
	mean	0.60	1.04	0.29
α^b/deg	Ni1	24.1	32.5	16.0
	Ni2	20.3		14.6
	Ni3	9.0		10.6
	mean	17.8	32.5	13.7
β^c/deg	Ni1	9.7	10.2	11.1
	Ni2	6.6		5.4
	Ni3	11.1		11.9
	mean	9.1	10.2	9.5
γ^d/deg	Ni1	23.4	35.6	6.6
	Ni2	17.2		17.5
	Ni3	19.2		8.1
	mean	19.9	35.6	10.7
$\varphi^{central\ e}$/deg	Ni1	15.7	25.8	9.6
	Ni2	15.0		12.3
	Ni3	5.5		15.1
	mean	12.1	25.8	12.3
$\varphi^{terminal\ f}$/deg	Ni1	1.9	3.6	12.1
	Ni2	5.5		3.1
	Ni3	2.2		10.5
	mean	3.2	3.6	8.6

[a] d is the shortest distance of a nickel ion from the best plane formed by the six carbon atoms of the central benzene ring of the phloroglucinol backbone. [b] α is the angle between the best planes of (1) N$_2$O$_2$ and (2) benzene of the central phloroglucinol backbone. [c] β is the angle between the best planes of (1) N$_2$O$_2$ and (2) benzene of the terminal phenolate. [d] γ is the angle between the best planes of (1) benzene of the central phloroglucinol backbone and (2) benzene of the terminal phenolate. [e] Bent angle Ni − X$_1^{central}$ − X$_2^{central}$. [f] Bent angle Ni − X$_1^{term}$ − X$_2^{term}$.

to the central N$_2$O$_2$ plane and relative to each other, and steps in the molecule caused by the two phenyl rings, which are nearly coplanar but with an offset.

As a result of the occurrence of all three kinds of distortions (helical, V-shaped, and step) in the nickel triplesalen complexes, the above-defined distance d is not a sufficient structural descriptor. A measure for the bending or folding of the ligands is provided by the angles between the N$_2$O$_2$ plane and the two benzene planes. Three different angles between the calculated best planes are summarized in Table 1. α is the angle between the N$_2$O$_2$ plane and the benzene plane of the central phloroglucinol backbone, whereas β is the angle between the N$_2$O$_2$ plane and the benzene plane of the terminal phenolate. γ is the angle between the benzene planes of the central phloroglucinol and the terminal phenolates. A close inspection of these values demonstrates that in all three complexes, the bending of the terminal phenolates is relatively small. The strong distortion in [(talen$^{t-Bu_2}$)Ni$^{II}_3$] mainly originates from a bending of the N$_2$O$_2$ planes with the central phloroglucinol benzene plane (α).

(40) Santos, I. C.; Vilas-Boas, M.; Piedale, M. F. M.; Freire, C.; Duarte, M. T.; de Castro, B. *Polyhedron* **2000**, *19*, 655.
(41) Azevedo, F.; de Carrondo, M. A. A. F.; de Castro, B.; Convery, M.; Domingues, D.; Freire, C.; Duarte, M. T.; Nielson, K.; Santos, I. C. *Inorg. Chim. Acta* **1994**, *219*, 43−54.
(42) Szlyk, E.; Wojtczak, A.; Larsen, E.; Surdykowski, A.; Neumann, J. *Inorg. Chim. Acta* **1999**, *293*, 239.
(43) (a) Wojtczak, A.; Szlyk, E.; Jaskolski, M.; Larsen, E. *Acta Chem. Scand.* **1997**, *51*, 274. (b) de Castro, B.; Freire, C.; Duarte, M. T.; Minas da Piedade, M. F.; Santos, I. C. *Acta Crystallogr., Sect. C* **2001**, *57*, 370.
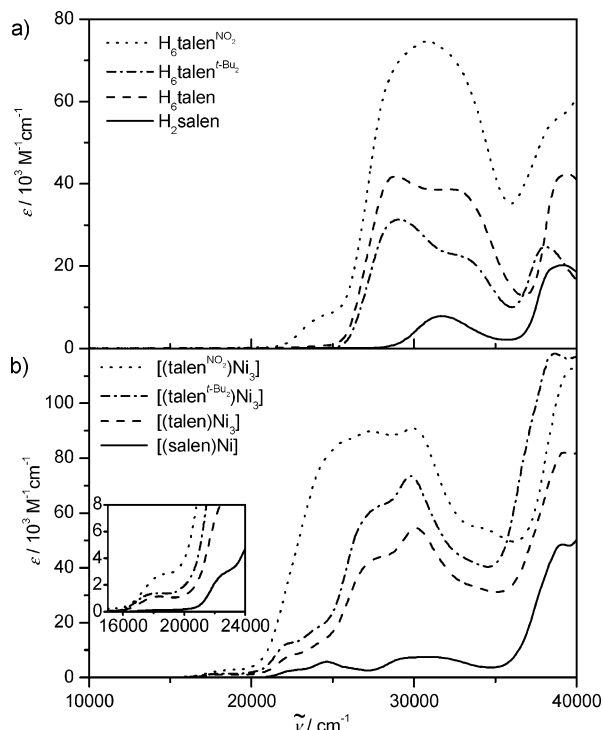
Scheme 4
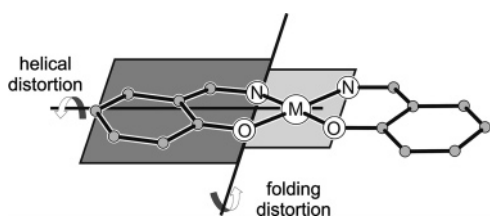
Although these angles provide more detailed information on the structural distortion as compared to that on the distance parameter d, they cannot differentiate between a helical and a folding distortion. Bending along an idealized line through neighboring N and O ligands leads to a folding of the N_2O_2 plane and the ligand plane, whereas bending along a line perpendicular to the former incorporating the Ni ion results in a helical distortion of the two planes (Scheme 4).

To differentiate between ligand folding and helical distortion, we calculated the bent angle φ (introduced by Cavallo and Jacobsen)[12] for the central Ni−phenolate units and for the terminal Ni−phenolate units (Table 1). The bent angle φ is defined by $\varphi = 180° - \angle(M-X_{NO}-X_R)$ (X_{NO} = midpoint of adjacent N and O donor atoms, X_R = midpoint of the six-membered chelate ring containing the N and O donor atoms). By this definition, the angle φ describes mainly the folding distortion and only minor effects of the helical distortion. A close inspection of the calculated values (Table 1) demonstrates that the folding of the terminal phenolates in $[(\text{talen})\text{Ni}^{II}_3]$ and $[(\text{talen}^{t-Bu_2})\text{Ni}^{II}_3]$ is relatively small and is somewhat larger in $[(\text{talen}^{NO_2})\text{Ni}^{II}_3]$. On the other hand, folding at the central phenolate units is more substantial in all three complexes. The folding at the central phenolate unit is twice as large for $[(\text{talen}^{t-Bu_2})\text{Ni}^{II}_3]$ as compared to that for $[(\text{talen})\text{Ni}^{II}_3]$ and $[(\text{talen}^{NO_2})\text{Ni}^{II}_3]$.

Electronic Absorption Spectroscopy. To get some insights into the variation of the electronic structure by going from a mononuclear salen complex to a trinuclear triplesalen complex, the electronic absorption spectra of the three ligands H_6talen, H_6talen$^{t-Bu_2}$, and H_6talen^{NO_2} and their trinuclear nickel complexes $[(\text{talen})\text{Ni}^{II}_3]$, $[(\text{talen}^{t-Bu_2})\text{Ni}^{II}_3]$, and $[(\text{talen}^{NO_2})\text{Ni}^{II}_3]$ were measured and compared to the spectra of the mononuclear model compounds H_2salen and $[(\text{salen})\text{Ni}^{II}]$. The comparison of the ligand spectra is shown in Figure 3a, and the comparison of the complex spectra is shown in Figure 3b. Spectral data are summarized in Table 2.

H_2salen exhibits a $\pi \rightarrow \pi^*$ transition involving the imine group around 32 000 cm^{-1}, whereas the absorptions above 36 000 cm^{-1} originate from $\pi \rightarrow \pi^*$ transitions associated with the phenolic chromophores.[44-46] The electronic spectrum of H_6talen displays absorption maxima at 46 500, 39 500, 32 400, and 28 800 cm^{-1}.[18] The energy and line shape of the high energy bands resembles that of H_2salen with an increase of the intensity by a factor of 2. This intensity increase is in accordance with a model of four noninteracting benzene moieties in H_6talen and two noninteracting benzene

(44) Bosnich, B. *J. Am. Chem. Soc.* **1968**, *90*, 627−632.
(45) Crawford, S. M. *Spectrochim. Acta* **1963**, *19*, 255−270.
(46) Di Bella, S.; Fragala, I.; Ledoux, I.; Diaz-Garcia, M. A.; Marks, T. J. *J. Am. Chem. Soc.* **1997**, *119*, 9550−9557.

Figure 3. (a) Electronic absorption spectra of H_2salen (CH$_3$CN), H_6talen (CH$_3$CN), H_6talen$^{t-Bu_2}$ (CH$_3$CN), and H_6talen^{NO_2} (CH$_2$Cl$_2$). (b) Electronic absorption spectra of $[(\text{salen})\text{Ni}^{II}]$ (CH$_3$CN), $[(\text{talen})\text{Ni}^{II}_3]$ (CH$_2$Cl$_2$), $[(\text{talen}^{t-Bu_2})\text{Ni}^{II}_3]$ (CH$_2$Cl$_2$), and $[(\text{talen}^{NO_2})\text{Ni}^{II}_3]$ (CH$_2$Cl$_2$). The inset shows the d−d transitions.

Table 2. Spectroscopic Properties of the Triplesalen Ligands and Their Trinuclear Nickel Complexes

H_2salen	H_6talen	H_6talen$^{t-Bu_2}$	H_6talen^{NO_2}
39 100 (20 000)	39 500 (42 000)	38 100 (24 700)	39 200 (sh)
31 600 (7900)	32 400 (39 000)	32 300 (sh)	30 800 (74 600)
	28 800 (42 000)	29 100 (31 300)	25 000 (sh)

$[(\text{salen})\text{Ni}^{II}]$	$[(\text{talen})\text{Ni}^{II}_3]$	$[(\text{talen}^{t-Bu_2})\text{Ni}^{II}_3]$	$[(\text{talen}^{NO_2})\text{Ni}^{II}_3]$
39 100 (48 500)	39 400 (82 000)	38 600 (118 000)	39 800 (112 000)
	33 700 (sh)	33 900 (sh)	33 900 (sh)
31 000 (7500)	30 000 (54 000)	29 800 (73 500)	30 000 (91 000)
28 600 (sh)	26 500 (sh)	28 100 (sh)	27 300 (90 000)
26 100 (sh)			
24 600 (6000)	24 300 (sh)	24 200 (sh)	26 100 (sh)
22 000 (sh)	21 800 (sh)	22 400 (sh)	
18 400 (140)	18 400 (1100)	18 200 (1400)	1900 (sh)

moieties in H_2salen. In contrast, the overall intensity in the 25 000−36 000 cm^{-1} region of H_6talen is roughly 10 times larger as compared to that of H_2salen. Instead of one $\pi \rightarrow \pi^*$ transition at 32 000 cm^{-1} in H_2salen, the spectrum of H_6talen exhibits two intense bands in this region at 32 400 and 28 800 cm^{-1}. The introduction of *tert*-butyl groups in H_6talen$^{t-Bu_2}$ does not alter the overall shapes and energies of the transitions in the absorption spectrum. However, the intensity is significantly decreased in H_6talen$^{t-Bu_2}$ (~66% of the intensity of H_6talen below 36 000 cm^{-1}). On the other hand, the nitro groups in H_6talen^{NO_2} cause an enormous intensity increase (~186% of the intensity of H_6talen below 36 000 cm^{-1}) but with slightly changed band shapes. The band shape of the strong absorption at 30 800 cm^{-1} indicates the superposition of several transitions. There is one ad-

ditional low-energy band around 25 000 cm^{-1}. These changes of the spectra due to the introduction of a nitro group are already evident in the spectrum of 4-nitrophenol as compared to the spectrum of phenol.

Thus, the electronic structure of a triplesalen ligand cannot be described as a 3-fold superposition of the electronic structure of a salen ligand. The topology of the triplesalen ligand with the shared, bridging phloroglucinol unit results in an electronic communication between the three salen subunits. This interaction may be described by an enlarged π system resulting in an increase of absorption intensity at lower energy. The intensity in this region and, thus, the electronic structure of the triplesalen ligands can be modulated by terminal substituents. Electron-donating groups (*tert*-butyl) yield an intensity decrease, whereas electron-withdrawing groups (nitro) result in an intensity increase.

The absorption spectrum of [(salen)Ni^{II}] consists of a weak band at 18 400 cm^{-1} and three resolved absorption features in the 21 000–27 000 cm^{-1} range where no transitions occur in the free ligand. Above 27 000 cm^{-1}, strong absorptions occur with counterparts in the spectrum of the free ligand. The two bands in the 27 000–35 000 cm^{-1} region originate from the first $\pi \rightarrow \pi^*$ transition of the free ligand (imine $\pi \rightarrow \pi^*$).[44] The band at 18 400 cm^{-1} was assigned as a d–d transition ($^1A_{1g} \rightarrow {}^1A_{2g}$; C_{2v} symmetry: $d_{xy} \rightarrow d_{x^2-y^2}$).[45,47] The three intense absorption features between 21 000 and 27 000 cm^{-1} are missing in the spectra of the free ligand and its zinc complex and have, therefore, been assigned to charge transfer (CT) transitions.[44] There are two possible types of CT transitions: (1) p $\rightarrow$ d ligand-to-metal CT (LMCT) transitions involving the p orbitals of the phenolate groups as donor orbitals and (2) d $\rightarrow \pi^*$ metal-to-ligand CT (MLCT) transitions involving the π^* orbitals of the imine groups as acceptor orbitals. Bosnich assigned the bands to d $\rightarrow \pi^*$ MLCT transitions.[44] This assignment is in agreement with the data of Elias and co-workers, who showed that these transitions do not occur in the corresponding tetrahydro salen complexes.[37] However, Marks and co-workers assigned these transitions as mixed LMCT and MLCT transitions because of the mixed character of the molecular orbitals and states involving C=N and O$_{2p}$ character.[46] The absence of any resonance enhancement of C–O stretches in the rR spectra of [(talen)Ni^{II}$_3$], [(talen$^{t-Bu_2}$)Ni^{II}$_3$], and [(talen^{NO_2})Ni^{II}$_3$] using an excitation wavelength of 413 nm (24 313 cm^{-1}; vide infra) argues against a strong contribution of phenolate LMCT to the transitions in this spectral region of the trinuclear complexes.

The spectrum of [(talen)Ni^{II}$_3$] exhibits strong absorption features above 35 000 cm^{-1} that are similar in shape and position to those of [(salen)Ni^{II}]. However, an assignment of spectral regions below 35 000 cm^{-1} to a specific kind of transition analogous to that observed in [(salen)Ni^{II}] (<21 000 cm^{-1}, d–d; 21 000–27 000 cm^{-1}, CT; 27 000–35 000 cm^{-1}, C=N π–π^*) is not evident in the spectrum of the trinuclear complex [(talen)Ni^{II}$_3$]. The spectral region from 25 000 to

35 000 cm^{-1} exhibits strong absorptions with a 10-fold intensity compared to the mononuclear model compound. As observed in the free ligand, this tremendous intensity increase is indicative of an electronic coupling between the three Ni–salen subunits through the bridging phloroglucinol backbone. The features between 20 000 and 25 000 cm^{-1} are reproduced in the trinuclear complex, indicating no drastic change in the imine MLCT as compared to the mononuclear complex. The intensity of the d–d transition (inset in Figure 3b) at 18 400 cm^{-1} is increased by a factor of 8 compared to that of the mononuclear model complex [(salen)Ni^{II}]. In D_{4h} symmetry, the ligand field transitions are all parity forbidden because of the presence of a center of inversion. The C_{2v} symmetry present in [(salen)Ni^{II}] removes the center of inversion, yielding a moderately strong d–d transition ($\epsilon \sim 110$ M^{-1}cm^{-1}). The observed intensity in the spectrum of [(talen)Ni^{II}$_3$] (1100 M^{-1}cm^{-1}) indicates a more pronounced symmetry lowering consistent with differences in the metal ligand bonding interaction of the two O/N donor sets (central vs terminal).

The effects on substitution observed in the spectra of the free ligands proceed in the spectra of the trinuclear nickel complexes. The spectrum of [(talen$^{t-Bu_2}$)Ni^{II}$_3$] resembles that of [(talen)Ni^{II}$_3$] with regard to band shapes and positions. The nitro group in [(talen^{NO_2})Ni^{II}$_3$] leads to a substantial increase of the absorbance at ca. 25 000 cm^{-1}, whereas the 30 000 cm^{-1} transition remains at largely the same position in all three Ni complexes. Thus, one may assign this latter absorption band to originate mainly from the π–π^* intraligand transition of the central phenolate, whereas the 27 000 cm^{-1} bands in [(talen)Ni^{II}$_3$] and [(talen$^{t-Bu_2}$)Ni^{II}$_3$] may result from the corresponding transition of the terminal phenolates that shifts to lower energy (ca. 25 000 cm^{-1}) in [(talen^{NO_2})-Ni^{II}$_3$].

The only difference between the spectra of the free ligands compared to the spectra of the complexes is a reversal of the intensity of the absorptions due to the *tert*-butyl substituents. Whereas in the ligand spectra, the intensity of H$_6$-talen is larger as compared to that of H$_6$talen$^{t-Bu_2}$, in the complex spectra, the intensity of [(talen$^{t-Bu_2}$)Ni^{II}$_3$] is larger as compared to that of [(talen)Ni^{II}$_3$].

In summary, the observed changes in the electronic absorption spectra by going from H$_2$salen to H$_6$talen, H$_6$talen$^{t-Bu_2}$, and H$_6$talen^{NO_2} and from [(salen)Ni^{II}] to [(talen)-Ni^{II}$_3$], [(talen$^{t-Bu_2}$)Ni^{II}$_3$], and [(talen^{NO_2})Ni^{II}$_3$] may be interpreted by a strong electronic communication between the three salen units involving π molecular orbitals. Whereas in the ligand spectra, intensities follow the trend of the electronic effects of the substituents (Hammett values), they do not in the spectra of the trinuclear complexes.

IR and rR Spectroscopy. In phenol and phenolate derivatives, the C–O stretching coordinate provides the dominant contribution to a mode in the region around 1250 cm^{-1}. This mode is IR active, and in the parent ligand H$_6$-talen, it can readily be assigned to a prominent band at 1279 cm^{-1}. The electron-donating *tert*-butyl groups shift this band by only 4 cm^{-1} to lower energy at 1275 cm^{-1}, but the electron-withdrawing nitro groups lead to a 22 cm^{-1} shift to

(47) (a) Ballhausen, C. J.; Liehr, A. D. *J. Am. Chem. Soc.* **1959**, *81*, 538–542. (b) Holm, R. H. *J. Am. Chem. Soc.* **1960**, *82*, 5632–5636. (c) Maki, G. *J. Chem. Phys.* **1958**, *29*, 1129–1138.

higher energy at 1297 cm^{-1}. The spectra of the free ligands do not provide any indication for two different C−O stretching modes, implying that the strength of the C−O bonds is essentially the same for the phloroglucinol and the terminal phenol moieties.

This finding is particularly surprising for the phenol derivatives carrying electron-donating (*tert*-butyl) and electron-withdrawing (NO$_2$) substituents in H$_6$talen$^{t-Bu_2}$ and H$_6$-talen^{NO_2}, respectively. It may be that intramolecular hydrogen bonds with the adjacent imine functions are different for the hydroxyl groups of phloroglucinol and the terminal phenols such that the effect of the ring substituents on the electron density of the C−O bonds is largely compensated. Additionally, only one band attributable to the C−O stretching can be identified in the Ni complexes (Figure S1, Supporting Information), implying that now the coordinative Ni−O bonds compensate the substituent effects on the C−O bonds. Furthermore, in all three complexes, these modes are at essentially the same frequency {[(talen)Ni$^{II}_3$], 1301 cm^{-1}; [(talen$^{t-Bu_2}$)Ni$^{II}_3$], 1299 cm^{-1}; [(talen^{NO_2})Ni$^{II}_3$], 1299 cm^{-1}}. Note that the frequencies are in the typical range of C−O stretchings in metal-coordinated phenolates (1280−1310 cm^{-1}).

In the rR spectra, excited at 413 nm (24 313 cm^{-1}), the C−O stretching modes cannot be detected, supporting the view that the electronic transitions between 23 000 and 25 000 cm^{-1} have little phenolate LMCT character (vide supra). Except for this mode, most of the prominent bands that are visible in the IR spectra are also detectable in the rR spectra and vice versa. Thus, resonance enhancement of the Raman bands does not appear to be restricted to a specific chromophoric part of the metal complex. Following the assignment of the electronic absorption bands, the excitation line is in rigorous resonance with the weak d → π* MLCT transitions involving the π* orbitals of the imine groups and in preresonance specifically with the substantially stronger π → π* intraligand transition of the terminal phenolates. Thus, one would expect that the modes that involve both the aromatic and the imine stretchings gain the strongest resonance enhancement. These modes are also likely to be IR active such that the appearance of the same modes in both the rR and the IR spectra can readily be understood. Pure imine stretching modes are usually observed at frequencies higher than 1650 cm^{-1}. For conjugated imines, somewhat lower frequencies down to 1620 cm^{-1} have been noted, as in the cases of retinalimines. For [(talen)Ni$^{II}_3$] and [(talen$^{t-Bu_2}$)Ni$^{II}_3$], no band can be detected in this region, implying that the double-bond character of the imine groups is weakened. Consequently, the C=N stretching coordinate may efficiently mix with the C−C stretching coordinates of the phenolates and, thus, contribute to the overlapping bands between 1530 and 1580 cm^{-1} that are partially only poorly resolved (Figure S1, Supporting Information). The rR spectrum of [(talen^{NO_2})Ni$^{II}_3$] displays a unique vibrational band pattern as it is dominated by the strong symmetric NO$_2$ stretching at 1321 cm^{-1}. This strong resonance enhancement is consistent with the assignment of the electronic absorption at ca. 25 000 cm^{-1} to a π → π* intraligand transition of the
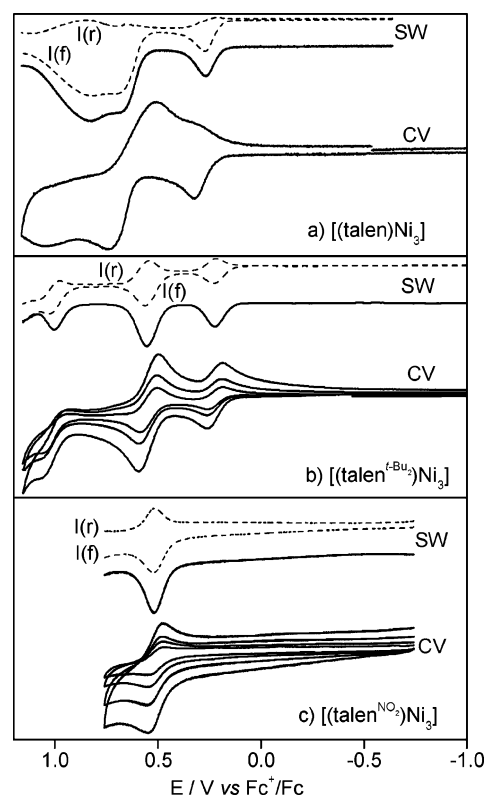
Figure 4. CVs and SWs in CH$_2$Cl$_2$ solution {0.10 M [N(*n*-Bu)$_4$]PF$_6$} at 20 °C recorded at a glassy carbon working electrode. (a) [(talen)Ni$^{II}_3$]: CV, scan rate 200 mV s^{-1}; SW, frequency 20 Hz. (b) [(talen$^{t-Bu_2}$)Ni$^{II}_3$]: CV, scan rates 50, 100, 200 mV s^{-1}; SW, frequency 10 Hz. (c) [(talen^{NO_2})-Ni$^{II}_3$]: CV, scan rates 25, 50, 100, 200 mV s^{-1}; SW, frequency 20 Hz.

NO$_2$-substituted phenolates. Thus, most of the bands in the spectrum are likely to originate from these aromatic rings. The band at 1551 cm^{-1} is assigned to the asymmetric NO$_2$ stretching that displays substantial IR activity. The second peculiarity of [(talen^{NO_2})Ni$^{II}_3$] refers to the aromatic C−C stretching region. Whereas both [(talen$^{t-Bu_2}$)Ni$^{II}_3$] and [(talen)Ni$^{II}_3$] display a single band at ca. 1615 cm^{-1} in the rR and IR spectra, two bands at 1606 and 1623 cm^{-1} are observed for [(talen^{NO_2})Ni$^{II}_3$]. This splitting suggests that the aromatic stretchings of the central and terminal phenolates do not appear at approximately the same frequency as those in [(talen$^{t-Bu_2}$)Ni$^{II}_3$] and [(talen)Ni$^{II}_3$]. However, NO$_2$ substitution does not affect the aromatic stretchings of only the terminal but also of the central ring.

Electrochemistry. Cyclic voltammograms (CVs) and square-wave voltammograms (SWs) of [(talen)Ni$^{II}_3$], [(talen$^{t-Bu_2}$)Ni$^{II}_3$], and [(talen^{NO_2})Ni$^{II}_3$] have been recorded in CH$_2$Cl$_2$ solutions containing 0.20 M [N(*n*-Bu)$_4$]PF$_6$ as a supporting electrolyte at a glassy carbon working electrode versus a Ag/AgNO$_3$ reference electrode. Small amounts of ferrocene were added after the completion of each set of experiments as an internal standard, and all potentials are referenced versus the Fc$^+$/Fc couple. Figure 4 shows the CVs and SWs of the three complexes, and redox potentials obtained from the voltammograms are compiled in Table 3.

The *tert*-butyl-substituted complex [(talen$^{t-Bu_2}$)Ni$^{II}_3$] exhibits three reversible oxidation waves at $E^1_{1/2} = 0.22$ V, $E^2_{1/2} = 0.55$ V, and $E^3_{1/2} = 1.00$ V (Figure 4b). Clearly, the

Table 3. Formal Electrode Potentials for Oxidation and Reduction (in V vs Fc$^+$/Fc) of Compounds [(talen$^{t-Bu_2}$)Ni$^{II}_3$], [(talen)Ni$^{II}_3$], and [(talen^{NO_2})Ni$^{II}_3$]^a

	oxidation			reduction
[(talen$^{t-Bu_2}$)Ni$_3$]	+1.00	+0.55	+0.22	
[(talen)Ni$_3$]	+1.05^{irr}	+0.73^{irr}	+0.32^{irr}	−2.10^{irr}
[(talen^{NO_2})Ni$_3$]		+1.16^{irr}	+0.52	−1.82^{irr}

^{a} Measured at ambient temperatures in solutions of CH$_2$Cl$_2$ containing 0.2 M [(n-Bu)$_4$N]PF$_6$. irr: redox process is irreversible; peak potentials are given.

peak currents of the wave at 0.55 V are twice as high as compared to the wave at 0.22 V. This indicates that the former represents a two-electron oxidation (which was confirmed by coulorimetric experiments, vide infra). Attempts to split this two-electron oxidation into two separate one-electron oxidations by low-temperature measurements and fast scan rates (up to 6 V s^{-1} at a microelectrode) failed. The CV wave of the third oxidation is distorted by irreversible oxidations that occur at higher potentials. However, inspection of the forward and reverse currents in the SW indicates that this third (one-electron) oxidation is reversible on the time scale of the CV and SW experiments.

The CV and SW of the parent complex [(talen)Ni$^{II}_3$] displays three oxidations too, at $E^1_{p,ox}$ = 0.32 V, $E^2_{p,ox}$ = 0.73 V, $E^3_{p,ox}$ = 1.05 V, but they are largely *irreversible*, because of the lack of the stabilizing bulky *tert*-butyl substituents (Figure 4a; $E_{p,ox}$ denotes the peak potentials for oxidation). The peak potentials of the second and third oxidation, coming off after an almost irreversible process, are not too reliable. However, it is apparent that the first oxidation of [(talen)Ni$^{II}_3$], which shows some reversibility, occurs at a potential 100 mV more positive than with [(talen$^{t-Bu_2}$)Ni$^{II}_3$], because the electron-donating properties of the *tert*-butyl groups facilitate oxidation.

The electronic effect of substituents is also seen with [(talen^{NO_2})Ni$^{II}_3$], where the first (reversible) oxidation is shifted, compared to [(talen)Ni$^{II}_3$], by 200 mV to the positive direction as a result of the electron-withdrawing NO$_2$ substituents, which impede oxidation. A second oxidative wave was observed with [(talen^{NO_2})Ni$_3$] too, but it was highly irreversible (at $E^2_{p,ox}$ = 0.82 V; not shown). Coulorimetric experiments established that the first oxidations of [(talen^{NO_2})-Ni$_3$] and of [(talen$^{t-Bu_2}$)Ni$_3$] are both one-electron processes.

At very negative potentials, there were highly irreversible reduction processes observed with [(talen)Ni$^{II}_3$] and [(talen^{NO_2})-Ni$^{II}_3$], at −2.1 and −1.8 V, respectively, which might be initiated by the Ni^{II}/Ni^I couple, but which will not be discussed further.

Spectroelectrochemistry. Controlled potential coulorimetric experiments have been performed (at −25 °C) at appropriate fixed potentials for the reversible electron-transfer waves of [(talen$^{t-Bu_2}$)Ni$^{II}_3$] and [(talen^{NO_2})Ni$^{II}_3$]. CVs and SWs before and after electrolysis were recorded and found to be identical. This confirms the reversibility of the systems and the stability of the oxidized species during the extended time period of electrolysis (1500 s). UV−vis spectra recorded in situ during electrolysis allowed for following the progress
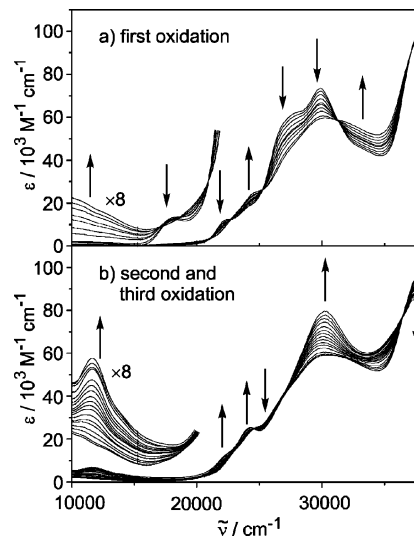
Figure 5. Controlled potential spectroelectrochemistry of (a) the one-electron oxidation of [(talen$^{t-Bu_2}$)Ni$^{II}_3$] at $E^1_{1/2}$ = 0.22 V and (b) the two-electron oxidation of [(talen$^{t-Bu_2}$)Ni$_3$]$^+$ at $E^2_{1/2}$ = 0.55 V at −25° C in CH$_2$Cl$_2$ solution {0.10 M [N(n-Bu)$_4$]PF$_6$}. The arrows indicate the observed spectral changes during the oxidations. Note that the spectra are not taken at a constant time interval but at a constant charge interval.
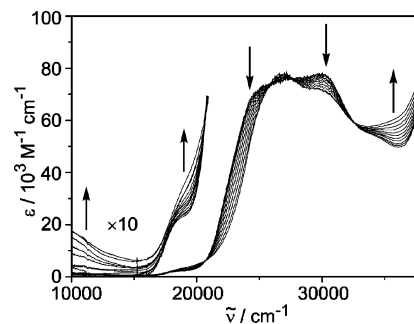
Figure 6. Controlled potential spectroelectrochemistry of the one-electron oxidation of [(talen^{NO_2})Ni$^{II}_3$] at $E^1_{1/2}$ = 0.52 in CH$_2$Cl$_2$ solution {0.10 M [N(n-Bu)$_4$]PF$_6$}. The arrows indicate the observed spectral changes during the oxidation. Note that the spectra are not taken at a constant time interval but at a constant charge interval.

of oxidation and for measuring the electronic spectra of the oxidized complexes.

The spectral changes that accompany the formation of the one-electron oxidized products [(talen$^{t-Bu_2}$)Ni$_3$]$^+$ (Figure 5a) and [(talen^{NO_2})Ni$_3$]$^+$ (Figure 6) are similar; the absorption bands in the 21 000−32 000 cm^{-1} range decrease and sharpen, and a new absorption band (ϵ > 2000 M^{-1} cm^{-1}) at low energies is formed (maximum below 10 000 cm^{-1}). Reasonably sharp isosbestic points demonstrate that no other species except the neutral form and the monocation is present {the two isosbestic points around 17 000 cm^{-1} observed with [(talen$^{t-Bu_2}$)Ni$_3$]$^+$ are not ideal, but here, the OD values are quite low}. The oxidations could be ligand-centered and generate phenoxyl radicals that possess characteristic absorption bands at 24 000−25 000 cm^{-1}. It is interesting that with both complexes, a slight increase in absorption in this range is observed upon oxidation {at 24 600 cm^{-1} with [(talen$^{t-Bu_2}$)-Ni$_3$]$^+$ and at 24 200 cm^{-1} with [(talen^{NO_2})Ni$_3$]$^+$}. However, it is only small, and the EPR measurements (vide infra) reveal unambiguously that at high temperatures, the predominant

forms of the monocations are Ni^{III} species. Therefore, these (weak) bands in the monocations must have a different origin.

Figure 5b shows the spectral changes associated with the two-electron oxidation of $[(talen^{t-Bu_2})Ni_3]^+$ to $[(talen^{t-Bu_2})Ni_3]^{3+}$. A strong absorption band around 30 300 cm^{-1} arises; the shoulder at 24 600 cm^{-1} observed in the monocation shifts to 24 200 cm^{-1} and increases in intensity, while an additional strong band in the low-energy range appears (at 11 700 cm^{-1}; $\epsilon = 7200$ M^{-1} cm^{-1}). The spectral changes follow the same pattern during the whole two-electron electrolysis under the formation of isosbestic points. There is no UV−vis-spectral indication for the appearance of a discrete $[(talen^{t-Bu_2})Ni_3]^{2+}$ species. This could indicate that the dication disproportionates because it is easier to oxidize than the trication; that is, it is mainly the trication and monocation that coexist in solution and generate the spectral changes.

$$2[(talen^{t-Bu_2})Ni_3]^{2+} \rightleftarrows$$
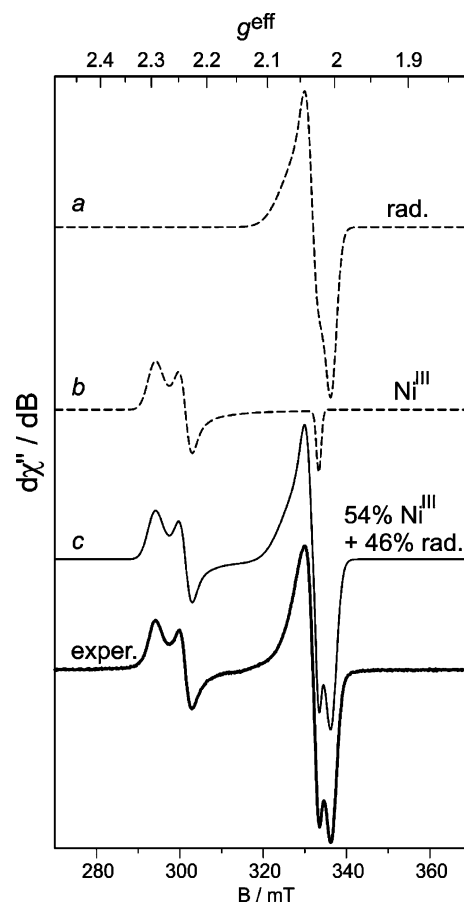$$[(talen^{t-Bu_2})Ni_3]^{3+} + [(talen^{t-Bu_2})Ni_3]^+$$
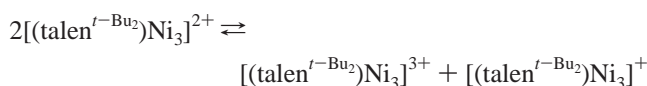
However, after oxidation with one electron per trinuclear monocation, the EPR signal of the monocation did not drop to one-half but was found to have largely decayed (vide infra). Therefore, the dication is expected to exist in solution, and the spectral changes in going from $[(talen^{t-Bu_2})Ni_3]^+$ to the dication and further to $[(talen^{t-Bu_2})Ni_3]^{3+}$ are purely additive, because the natures of the (independent) oxidation processes are the same for the dication and trication. Since no radical signal was observed with the trication by EPR spectroscopy at low temperatures, the two oxidations may both be nickel-centered, or they are ligand centered and tautomerize to a Ni^{III} species at low temperatures, similarly as observed in the oxidized monomeric complex [(salen′)-Ni]$^+$.[48]

EPR Spectroscopy. The neutral complexes [(talen)Ni^{II}₃], [(talen$^{t-Bu_2}$)Ni^{II}₃], and [(talen^{NO_2})Ni^{II}₃] are EPR silent because of the diamagnetism of square-planar coordinated Ni^{II} (d^8, $S = 0$). In contrast, the electrochemically generated oxidized forms of [(talen$^{t-Bu_2}$)Ni₃] and [(talen^{NO_2})Ni₃] are EPR active. The X-band EPR spectrum of [(talen$^{t-Bu_2}$)Ni₃]$^+$ measured at 10 K under nonsaturating conditions consists of two sub-spectra, as shown in Figure 7. Deconvolution and simulation clearly establishes that two $S = 1/2$ species are present. One subspectrum (54% intensity, trace b) exhibits a strong g anisotropy (2.294, 2.238, 2.023) with severe deviation from g_e, whereas the other subspectrum (46%, trace a) exhibits a nearly isotropic g tensor (2.065, 2.036, 2.006) close to g_e. The former spectrum belongs to a metal-oxidized Ni^{III} (d^7, $S = 1/2$) species with a (d$_{z^2}$)^1 ground state[41,49] and the latter to a ligand-oxidized radical species. The observed deviation from 2.0023 demonstrates that this radical is coordinated to a diamagnetic Ni^{II} ion. The covalent overlap of the radical p orbitals with the metal orbitals results in some spin−orbit coupling and, thus, to the deviation from 2.0023.

(48) Shimazaki, Y.; Tani, F.; Fukui, K.; Naruta, Y.; Yamauchi, O. *J. Am. Chem. Soc.* **2003**, *125*, 10512−10513.
(49) Freire, C.; de Castro, B. *J. Chem. Soc., Dalton Trans.* **1998**, 1491−1497.
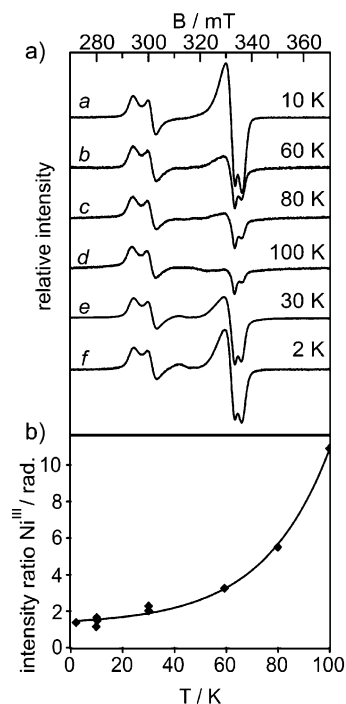
Figure 7. X-band EPR spectrum of electrogenerated [(talen$^{t-Bu_2}$)Ni₃]$^+$ in frozen CH₂Cl₂ at 10 K. Conditions: microwave frequency, 9.4372 GHz; modulation amplitude, 12 G; power, 50.4 μW. See the text for details of the simulation (traces $a-c$).

The ratio of the Ni^{III}-to-radical subspectra is temperature-dependent (Figure 8). By increasing the temperature, the intensity of the radical species reversibly decreases and vice versa (Figure 8a).[50] For each temperature, careful inspections of the power dependencies of the spectra have been performed to avoid saturation or rapid passage effects. The interconversion of the Ni^{III} species to the radical species shows a temperature-dependent equillibrium in the measured temperature range 4−100 K. The intensity ratio of Ni^{III} and radical spectra was determined from the simulation of a series of spectra, as shown in Figure 8a, for example, by using the same g tensor and line widths parameters taken from the 10 K measurement throughout. The result is depicted in Figure 8b.

Figure 9 displays the EPR spectral changes associated with the oxidation of [(talen$^{t-Bu_2}$)Ni₃] to the trication [(talen$^{t-Bu_2}$)-Ni₃]$^{3+}$. The spectrum of the monocation has been analyzed in detail above. The spectrum of the dication [(talen$^{t-Bu_2}$)Ni₃]$^{2+}$ was obtained after a roughly one-electron oxidation equivalent of the two-electron oxidation at $E^2_{1/2} = 0.55$ V was consumed. Overall, the spectrum of the dication [(talen$^{t-Bu_2}$)-Ni₃]$^{2+}$ exhibits much weaker intensity, in accordance with a

(50) Some decomposition of the oxidized species [(talen$^{t-Bu_2}$)Ni₃]$^+$ is observed during the temperature cycle with a signal of the decomposition product around $g = 2.1$.

Figure 8. (a) Temperature dependence of the X-band EPR spectra of electrogenerated [(talen$^{t-Bu_2}$)Ni$_3$]$^+$ in frozen CH$_2$Cl$_2$. The spectra have been measured with increasing and decreasing temperature in the order of trace *a* to trace *f*. The intensities are normalized to the intensity of the Ni^{III} signal at *g* = 2.3 to emphasize the reversible radical signal decrease by increasing temperature and vice versa. (b) Temperature dependence of the Ni^{III}-to-radical ratio obtained by simulation of the X-band EPR spectra. The solid line is an exponential curve serving as a guide for the eyes.
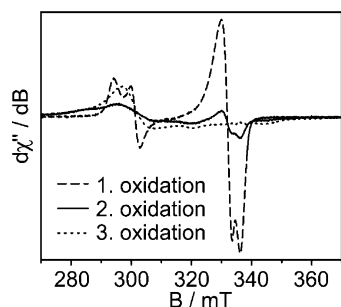
Figure 9. X-band EPR spectrum of electrogenerated [(talen$^{t-Bu_2}$)Ni$_3$]$^+$, [(talen$^{t-Bu_2}$)Ni$_3$]$^{2+}$, and [(talen$^{t-Bu_2}$)Ni$_3$]$^{3+}$ in frozen CH$_2$Cl$_2$ at 10 K. Conditions for [(talen$^{t-Bu_2}$)Ni$_3$]$^+$: microwave frequency, 9.4372 GHz; modulation amplitude, 12 G; power, 50.4 μW. For [(talen$^{t-Bu_2}$)Ni$_3$]$^{2+}$: microwave frequency, 9.4368 GHz; modulation amplitude, 12 G; power, 50.4 μW. For [(talen$^{t-Bu_2}$)Ni$_3$]$^{3+}$: microwave frequency, 9.4370 GHz; modulation amplitude, 12 G; power, 50.4 μW. Note that the use of one set of experimental conditions allows the direct comparison of the amplitudes.

formal integer spin system probably due to spin coupling. The main contribution is a broad spectrum with *g* values of 2.37, 2.24, and 2.11. A weak radical signal due to the presence of some monocation [(talen$^{t-Bu_2}$)Ni$_3$]$^+$ is still detectable. The spectrum of the fully oxidized species [(talen$^{t-Bu_2}$)Ni$_3$]$^{3+}$ gains in intensity (formally a half-integer spin system). The radical species has disappeared completely, and a broad signal with *g* values of 2.28, 2.25, and 1.96 is detectable.

Figure 10 shows the X-band EPR spectrum at 10 K of electrochemically generated [(talen^{NO_2})Ni$_3$]$^+$. The similarity to the analogous spectrum of the *tert*-butyl-substituted
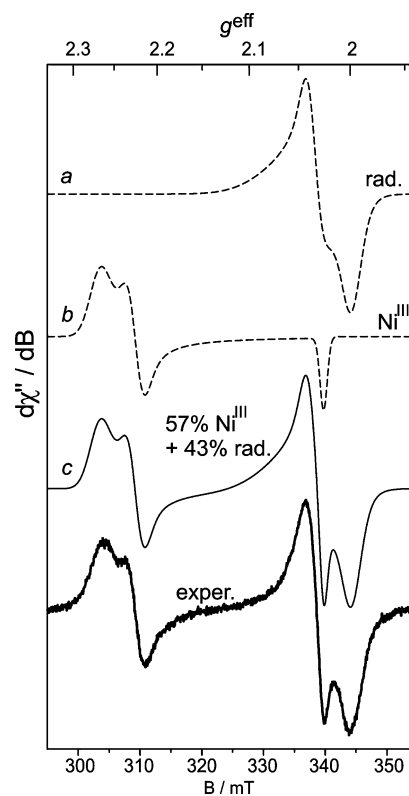
**Figure 10.** X-band EPR spectrum of electrogenerated [(talen^{NO_2})Ni$_3$]$^+$ in frozen CH$_2$Cl$_2$ at 10 K. Conditions: microwave frequency, 9.6310 GHz; modulation amplitude, 10 G; power, 200.2 μW. See the text for details of the simulation (traces *a*–*c*).

monocation [(talen$^{t-Bu_2}$)Ni$_3$]$^+$ is remarkable. Consequently, deconvolution and simulation confirms the presence of two $S = 1/2$ species. The Ni^{III} subspectrum (57% intensity, trace b) is characterized by an anisotropic *g* tensor (2.268, 2.225, 2.026), whereas the radical subspectrum (43%, trace a) shows a nearly isotropic *g* tensor (2.062, 2.037, 2.001). This striking similarity in the EPR spectra of [(talen$^{t-Bu_2}$)Ni$_3$]$^+$ and [(talen^{NO_2})Ni$_3$]$^+$ is an unambiguous proof for the similarity of their electronic structures, in particular, the site of oxidation and the degree of delocalization, whereas the slight differences in the *g* tensors demonstrate the influence of the terminal substituents on the electronic structures of the metal sites.

Discussion

Variation of the Electronic Structure of the Triplesalen Complexes by Changes in the Substituents of the Terminal Phenolates. The stepwise assembly of the triplesalen ligands based on the isolation of the triplesalen half unit **2** opens the opportunity to easily introduce, in the last step, different terminal phenoles. Thus, a control over the electronic properties of trinuclear complexes may be envisioned by the electronic properties on the substituents of the terminal phenolates. A useful objective would be the possibility to control the electronic communication of the three coordinated metal ions in a trinuclear triplesalen complex. This control would allow an optimization of the cooperative interaction between the metal ions in catalysis and, in particular, the ability to tune the exchange coupling in paramagnetic

Scheme 5
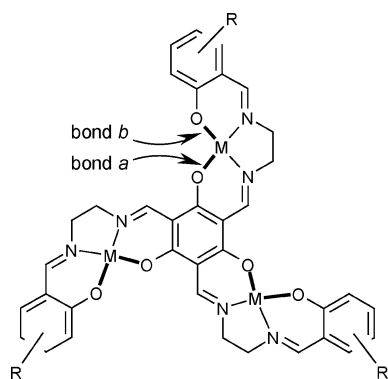
complexes. As the electronic communication between the three metal ions is mediated by the central metal–phenolate bonds (bonds *a* in Scheme 5), a strengthening of these bonds would increase the interaction between the metal ions. An indirect handle for influencing the central metal–phenolate bonds *a* is provided by a variation of the terminal metal–phenolate bonds (bonds *b* in Scheme 5). In accordance with Pauling's electroneutrality principle, a weakening of the terminal bonds *b* would strengthen the central bonds *a* and vice versa. This indirect manipulation of the covalency of a specific metal–ligand bond by changes in the electronic characteristics of the remaining metal–ligand bonds has been experimentally quantified by ligand K edge X-ray absorption spectroscopy.[51] In this respect, the introduction of the *tert*-butyl groups ($H_6talen^{t-Bu_2}$) should lead to stronger bonds *b* and weaker bonds *a* as compared to those of complexes of the parent ligand H_6talen, whereas the use of the nitro groups ($H_6talen^{NO_2}$) should result in weaker bonds *b* and, thus, stronger bonds *a*.

The comparison of the electronic absorption spectra of the mononucleating salen ligand to the spectra of the trinucleating triplesalen ligands demonstrates a strong intensity increase below 36 000 cm^{-1} indicative of an increased π system. The intensity in this region and, thus, the electronic structures of the triplesalen ligands are modulated by the terminal substituents. Electron-donating groups (*tert*-butyl) yield an intensity decrease, whereas electron-withdrawing groups (nitro) result in an intensity increase. These results are in accordance with the measured reduction potentials for the $[(talen^X)Ni_3]^+ + e^- \rightarrow [(talen^X)Ni_3]$ electron-transfer process. The potential of the parent $[(talen)Ni_3]$ complex of 0.32 V versus Fc$^+$/Fc is cathodically shifted to 0.22 V versus Fc$^+$/Fc in $[(talen^{t-Bu_2})Ni_3]$ because of the introduction of the *tert*-butyl groups, whereas the introduction of a nitro group results in an anodic shift to 0.52 V versus Fc$^+$/Fc in $[(talen^{NO_2})Ni_3]$. Thus, the overall electron density in the redox active orbitals has been modulated by the terminal substituents. The trends in the redox potential and in the absorption intensity follow the trend in the respective Hammett values.

The increased intensity of the d–d transitions in the trinuclear nickel triplesalen complexes as compared to that in the mononuclear nickel salen complex reflects the asym-

metry in the nature of the nickel phenolate bonding between the central bonds *a* and the terminal bonds *b*. Additionally, the absorption features between 20 000 and 25 000 cm^{-1} are reproduced in the trinuclear complexes, indicating no drastic change in the imine MLCT as compared to that of the mononuclear complex.

However, the trend observed in the absorption spectra of the free ligands is not reproduced in the absorption spectra of the trinuclear complexes where the intensity follows the trend R = H < *tert*-butyl < NO$_2$. This trend indicates that, besides the control by the electron density on the terminal phenolates, a further effect modulates the electronic structure of the trinuclear complexes.

The comparison of the Ni–O distances provides an additional argument that the electronic structure in the trinuclear complexes is modulated by a further effect. The short bond *a* (1.82 Å) in comparison to the long bond *b* (1.86 Å) in the parent complex $[(talen)Ni^{II}_3]$ reflects the intrinsic difference in the covalency of the Ni–OPh bonds due to the asymmetry between a central and a terminal phenolate. The shortening of bond *b* (1.84 Å) accompanied by the lengthening of bond *a* (1.84 Å) in the *tert*-butyl derivative $[(talen^{t-Bu_2})Ni^{II}_3]$ may be attributed to the electronic effects of the terminal electron-donating groups. However, the small decrease in the length of bond *b* (1.85 Å) in the nitro derivative $[(talen^{NO_2})Ni^{II}_3]$ accompanied by no significant effect on bond *a* as compared to the parent complex $[(talen)-Ni^{II}_3]$ is a clear indication that the nickel phenolate bonding is not only mediated by the nature of the terminal phenolates. This is especially true when taking into account that a nitro group induces stronger effects as compared to a *tert*-butyl group (vide supra).

We attribute this additional effect to a change in the orientation of the phenolate p orbitals relative to the nickel d orbitals by ligand folding imposing a change in the nickel–phenolate bonding. A detailed analysis of the ligand folding reveals that the bending of the terminal phenolates in $[(talen)-Ni^{II}_3]$ and $[(talen^{t-Bu_2})Ni^{II}_3]$ is relatively small and that it is somewhat larger in $[(talen^{NO_2})Ni^{II}_3]$. On the other hand, folding at the central phenolate units is more substantial in all three complexes. The bending at the central phenolate unit is twice as large for $[(talen^{t-Bu_2})Ni^{II}_3]$ as the folding for $[(talen)Ni^{II}_3]$ and $[(talen^{NO_2})Ni^{II}_3]$. These geometrical changes modulate the nickel–phenolate bonding. One of the three p orbitals of a phenolic oxygen atom is mainly involved in the strong C$_{ar.}$–O bond. In a planar arrangement of the phenol ring relative to the N$_2$O$_2$ coordination plane with generally observed C–O–Ni angles of $\sim$125–130°, one of the remaining O p orbitals is used for a pseudo σ bond to the metal and the second for a π bond to the metal.[51] Folding of the ligand leads to a situation where a strict distinction of σ and π bonding is not feasible anymore. The overlap of the oxygen pseudo σ orbital with the Ni^{II} d$_{x^2-y^2}$ orbitals decreases, whereas an overlap of the oxygen π orbitals with the Ni^{II} d$_{x^2-y^2}$ orbitals develops upon ligand bending. Thus, the strong bending at the central phenolate in $[(talen^{t-Bu_2})Ni^{II}_3]$ opens an overlap of the phenolate π orbital with the Ni d$_{x^2-y^2}$ orbital that is absent in the nearly planar arrangement of

(51) Glaser, T.; Hedman, B.; Hodgson, K. O.; Solomon, E. I. *Acc. Chem. Res.* **2000**, *33*, 859–868.

[(talen^{NO_2})Ni$^{II}_3$]. This additional π-conjugation pathway is evidenced by the stronger absorption intensity in the spectrum of [(talen$^{t-Bu_2}$)Ni$^{II}_3$], as it was expected by comparison to the spectra of the free ligands.

In summary, two opposing effects mediate the central nickel−phenolate bonding and, thus, the electronic communication between the nickel ions: (a) The introduction of *tert*-butyl (nitro) groups weakens (strengthens) the central nickel−phenolate bonds *a* because of a change of the covalency of the terminal phenolate bonds *b,* and (b) the introduction of the *tert*-butyl (nitro) groups results in a folding (no folding) of the ligand, opening a new bonding pathway (no new bonding pathway) that strengtens (weakens) the central nickel−phenolate bonds *a.*

Valence Tautomerism in the Oxidized [(talen^x)Ni$_3$]$^+$ Species. The electrochemistry of mononuclear nickel salen complexes has been intensively studied.[41,49,52] The parent complex [(salen)Ni] shows a reduction at low potentials of ~ -2 V versus Fc$^+$/Fc and an oxidation around 0.5 V versus Fc$^+$/Fc. Whereas the reductive wave shows a reversible behavior independent of the solvent used, the oxidative wave shows a reversible behavior only in solvents with good donor capability and an irreversible behavior in solvents that interact only weakly with metal ions. The current of the irreversible waves increases during consequent sweeps. This behavior was attributed to a Ni^{II} to Ni^{III} oxidation in good donor solvents with stabilization of the high oxidation state by concomitant increase of the coordination number, whereas in poorly coordinating solvents, the oxidation process is ligand-centered. The ligand-centered oxidation initiates an oxidative polymerization at the electrode surface. Methyl substitution at the para position inhibits polymerization, whereas methyl substitution at the ortho postion only does not. One may conclude that oxidation occurs regardless of the solvent, at first, at the nickel ion, which is either stabilized by a donor solvent or oxidizes, in a second step, the ligand in the absence of stabilizing donor solvents. For complexes of ortho- and para-substituted salen ligands, two oxidative waves may be resolved that have been assigned to a Ni^{III} oxidation followed by an additional ligand oxidation. The electrochemically generated complex [(salen′)Ni]$^+$ exhibits a temperature-dependent equilibrium between a metal-oxidized and a ligand-oxidized species. At −150 °C, the EPR spectrum shows only the typical signal of a Ni^{III} species (g_1 = 2.30, g_2 = 2.23, g_3 = 2.02, g_{eff} = 2.18), whereas at −80 °C, only that of a phenoxyl radical species is present (g_{iso} = 2.04).[48]

It is interesting to compare these results with the oxidation process of the trinuclear nickel triplesalen complexes. Electrochemically generated [(talen$^{t-Bu_2}$)Ni$_3$]$^+$ displays, at 10 K, the EPR spectra of a Ni^{III} species (g_1 = 2.30, g_2 = 2.24, g_3 = 2.02, g_{eff} = 2.19) and of a ligand-centered radical species (g_{iso} = 2.04). The ratio of these two species is temperature-dependent. Such isomeric species with spectroscopically well-defined differences in their charge distributions have been called valence tautomers.[53] In contrast to the mononuclear complex [(salen′)Ni]$^+$, in the trinuclear complex [(talen$^{t-Bu_2}$)Ni$_3$]$^+$, the radical signal disappears with increasing temperature, giving rise to a pure Ni^{III} species at higher temperatures. A strong band at 9070 cm^{-1} (ϵ = 3000 M^{-1} cm^{-1}) in [(salen′)Ni]$^+$ was assigned to an intervalence transition. Analogous intense bands below 10 000 cm^{-1} have also been detected in the trinuclear oxidized species.

The EPR spectrum of [(talen^{NO_2})Ni$_3$]$^+$ at 10 K also displays two subspectra, and their parameters as well as the ratio of the two subspectra are close to those of [(talen$^{t-Bu_2}$)Ni$_3$]$^+$. Thus, the electronic structures of the two oxidized species [(talen^{NO_2})Ni$_3$]$^+$ and [(talen$^{t-Bu_2}$)Ni$_3$]$^+$ are strongly related. This is a clear indication that the radical species is associated with the central benzene of the phloroglucinol backbone. Terminal phenoxyl radicals would display different EPR spectra for [(talen$^{t-Bu_2}$)Ni$_3$]$^+$ and [(talen^{NO_2})Ni$^{II}_3$]$^+$.

The concomitant detection of both valence tautomers (radical and Ni^{III} species) and their temperature-dependent interconversion in the trinuclear complexes [(talen$^{t-Bu_2}$)Ni$_3$]$^+$ and [(talen^{NO_2})Ni$^{II}_3$]$^+$ as well as in the mononuclear complex [(salen′)Ni]$^+$ indicates that these pairs of valence tautomers have comparable energies, that is, quasi-degenerate ground states.[54] The temperature dependence of the equilibrium is considered to be entropy driven.[55] In the well-established cobalt dioxolene valence tautomer systems,[56] the main contribution of the entropy change is associated with a change in the cobalt−ligand bond length as a result of occupation of cobalt σ* antibonding orbitals and a higher density of vibrational levels.[54,55] In the case of the nickel triplesalen (as well as salen) systems, the two valence tautomers are associated with either Ni^{II} low spin (d$_{z^2}$)^2 or Ni^{III} low spin (d$_{z^2}$)^1. The d$_{z^2}$ orbital is not directed to a ligand and is, thus, overall nonbonding in nature. Thus, no dramatic change in the bond lengths is expected for the two forms, and the vibrational entropic driving force should be reduced.

In the mononuclear complex [(salen′)Ni]$^+$, the Ni^{III} species is energetically favored at low energies and the radical species is entropically favored at higher temperatures.[48] This entropy gain might be associated with the two possible phenoxyl radical species that are energetically degenerated. However, in the trinuclear species [(talen$^{t-Bu_2}$)Ni$_3$]$^+$ and [(talen^{NO_2})Ni$^{II}_3$]$^+$, the Ni^{III} species is not energetically favored compared to the radical species. This might be attributed to

(52) (a) Kapturkiewicz, A.; Behr, B. *Inorg. Chim. Acta* **1983**, *69*, 247−251. (b) Opallo, M.; Behr, B.; Kapturkiewicz, A. *J. Electroanal. Chem.* **1985**, *162*, 427−432. (c) Goldsby, K. A.; Blaho, J. K.; Hoferkamp, L. A. *Polyhedron* **1989**, *8*, 113−115. (d) Böttcher, A.; Elias, H.; Jäger, E.-G.; Langfelderova, H.; Mazur, M.; Müller, L.; Paulus, H.; Pelikan, P.; Rudolph, M.; Valko, M. *Inorg. Chem.* **1993**, *32*, 4131−4138. (e) Leung, W.-H.; Chan, E. Y. Y.; Chow, W. K. F.; Williams, I. D.; Peng, S.-M. *J. Chem. Soc., Dalton Trans.* **1996**, 1229−1236. (f) Vilas-Boas, M.; Freire, C.; de Castro, B.; Christensen, P. A.; Hillmann, A. R. *Inorg. Chem.* **1997**, *36*, 4919−4929.

(53) Buchanan, R. M.; Pierpont, C. G. *J. Am. Chem. Soc.* **1980**, *102*, 4951−4957.

(54) (a) Dei, A.; Gatteschi, D.; Sangregorio, C.; Sorace, L. *Acc. Chem. Res.* **2004**, *37*, 827−835. (b) Shultz, D. A. In *Magnetism: Molecules to Materials*; Miller, J.-S., Drillon, M., Eds.; Wiley-VCH: Weinheim, Germany, 2001; Vol. II, pp 281−306.

(55) Adams, D. M.; Dei, A.; Rheingold, A. L.; Hendrickson, D. N. *J. Am. Chem. Soc.* **1993**, *115*, 8221−8229.

(56) (a) Pierpont, C. G.; Lange, C. W. *Prog. Inorg. Chem.* **1994**, *41*, 331−442. (b) Pierpont, C. G. *Coord. Chem. Rev.* **2001**, *216*, 99−125.

a class III delocalization[57] of the central phenoxyl radical Ni^{II} species over all three phenolate Ni^{II} sites. The entropy gain associated with the Ni^{III} species might then be attributed to the degeneracy of the three sites for the Ni^{III} oxidation. Thus, the mixed valence Ni^{III} Ni^{II} Ni^{II} form should be of class II.[57]

Conclusions

We have synthesized a series of triplesalen ligands that bridge three salen coordination environments in a *meta*-phenylene arrangement by a common phloroglucinol backbone. The hexa-anionic forms are triple tetradentate ligands and are capable of coordinating three transition metal ions, as demonstrated by the synthesis of their trinuclear nickel complexes. The three nickel−salen subunits are electronically conjugated through the π system of the central phloroglucinol unit, which might be useful for cooperative effects in catalysis. Moreover, the *tert*-butyl-substituted complex [(talen$^{t-Bu_2}$)Ni$^{II}_3$] forms a chiral half bowl. The interconversion between the two racemic forms is fast on the NMR time scale. However, the use of enantiomeric pure diimine moieties or the application of Katsuki's concept to convert enantiomeric conformations of an achiral salen complex to diastereomeric forms by interaction with a chiral ligand[58] are options for the application of the trinuclear triplesalen complexes in enantioselective processes. The comparison of the efficiency of a chiral pocket formed by a mononuclear salen complex to a chiral half bowl created by a triplesalen ligand in enantioselective catalysis is currently being pursued.

The oxidized trinuclear nickel triplesalen complexes are intrinsically mixed valence because of three nickel−salen subunits. Additionally, this oxidized species exhibits a valence tautomerism between a metal-centered oxidation to Ni^{III} and a ligand-centered oxidation to a phenoxyl radical. The comparison between [(talen$^{t-Bu_2}$)Ni$_3$]$^+$ and [(talen^{NO_2})-Ni$_3$]$^+$ establishes that the ligand-centered oxidation occurs at the central benzene ring. The delocalization of this phenoxyl radical over three nickel−phenolate subunits stabilizes this radical compared to the analogous phenoxyl radical of a mononuclear [(salen′)Ni]$^+$. This delocalization proves the strong electronic communication of the three nickel−salen subunits through the central phloroglucinol unit. The use of paramagnetic transition-metal ions with a triplesalen ligand is currently being pursued in our laboratory.

Supporting Information Available: Complete single-crystal X-ray diffraction details in CIF format. FTIR and rR spectra of the trinuclear complexes (Figure S1) and interatomic distances and angles (Table S1). This material is available free of charge via the Internet at http://pubs.acs.org.

IC050268X

(57) Robin, M. B.; Day, P. *Adv. Inorg. Chem. Radiochem.* **1967**, *10*, 247−422.
(58) (a) Hashihayata, T.; Ito, Y.; Katsuki, T. *Synlett* **1996**, 1079−1081. (b) Hashihayata, T.; Ito, Y.; Katsuki, T. *Tetrahedron* **1997**, *53*, 9541−9552. (c) Miura, K.; Katsuki, T. *Synlett* **1999**, 783−785.